Inorg. Chem. **2008**, *47*, 1532−1547

Platinum(II) Diimine Complexes with Catecholate Ligands Bearing Imide Electron-Acceptor Groups: Synthesis, Crystal Structures, (Spectro)Electrochemical and EPR studies, and Electronic Structure

Nail M. Shavaleev,[†] E. Stephen Davies,[‡] Harry Adams,[†] Jonathan Best,[†] and Julia A. Weinstein*[,†]

Department of Chemistry, University of Sheffield, Sheffield, S3 7HF, United Kingdom, School of Chemistry, University of Nottingham, Nottingham NG7 2RD, United Kingdom

Received September 14, 2007

A series of catechols with attached imide functionality (imide = phthalimide PHT, 1,8-naphthalimide NAP, 1,4,5,8-naphthalenediimide NDI, and NAP-NDI) has been synthesized and coordinated to the Pt^{II}(bpy*) moiety, yielding Pt(bpy*)(cat-imide) complexes (bpy* = 4,4′-di-*tert*-butyl-2,2′-bipyridine). X-ray crystal structures of PHT and NAP complexes show a distorted square-planar arrangement of ligands around the Pt center. Both complexes form "head-to-tail" dimers in the solid state through remarkably short unsupported Pt···Pt contacts of 3.208 (PHT) and 3.378 Å (NAP). The Pt(bpy*)(cat-imide) complexes are shown to combine optical (absorption) and electrochemical properties of the catecholate (electron-donor) and imide (electron-acceptor) groups. The complexes show a series of reversible reduction processes in the range from −0.5 to −1.9 V vs Fc^+/Fc, which are centered on either bpy* or imide groups, and a reversible oxidation process at +0.07 to +0.14 V, which is centered on the catecholate moiety. A combination of UV−vis absorption spectroscopy, cyclic voltammetry, UV−vis spectroelectrochemistry, and EPR spectroscopy has allowed assignment of the nature of frontier orbitals in Pt(bpy*)(cat-imide) complexes. The HOMO in Pt(bpy*)(cat-imide) is centered on the catechol ligand, while the LUMO is localized either on bpy* or on the imide group, depending on the nature of the imide group involved. Despite the variations in the nature of the LUMO, the lowest-detectable electronic transition in all Pt(bpy*)(cat-imide) complexes has predominantly ligand-to-ligand (catechol-to-diimine) charge-transfer nature (LLCT) and involves a bpy*-based unoccupied molecular orbital in all cases. The LLCT transition in all Pt(bpy*)(cat-imide) complexes appears at 530 nm in CH_2Cl_2 and is strongly negatively solvatochromic. The energy of this transition is remarkably insensitive to the imide group present, indicating lack of electronic communication between the imide and the catechol moieties within the cat-imide ligand. The high extinction coefficient, $\sim 6 \times 10^3$ L mol^{-1} cm^{-1} of this predominantly LLCT transition is the result of the Pt orbital contribution, as revealed by EPR spectroscopy of the complexes in various redox states. The CV profile of the oxidation process of Pt(bpy*)(cat-imide) in CH_2Cl_2 and DMF is concentration dependent, as was shown for NDI and PHT complexes as typical examples. Oxidation appears as a simple diffusion-limited process at low concentrations, with an increasing anodic-to-cathodic peak separation eventually resolving as two independent consecutive waves as the concentration of the complex increases. It is suggested that aggregation of the complexes in the diffusion layer in the course of oxidation is responsible for the observed concentration dependence. Overall, the Pt(bpy*)(cat-imide) complexes are electrochromic compounds in which a series of stepwise reversible redox processes in the potential range from 0.2 to −2 V (vs Fc^+/Fc) leads to tuneable absorbencies between 300 and 850 nm.

Introduction

The aromatic acid imides are chemically and photo stable compounds that are used widely as pigments, luminescent materials, and solar energy harvesters.[1–4] A combination of strong electron-accepting properties with the stability of the radical anions formed upon reversible reductions and the unique spectroscopic signature of each of the individual redox states[3,5,6] led to the extensive use of the imides as components in extended organic and metal-based assemblies for photoinduced charge separation.[7,8] An incorporation of

* To whom correspondence should be addressed. E-mail: Julia.Weinstein@sheffield.ac.uk.
[†] University of Sheffield.
[‡] University of Nottingham.

10.1021/ic701821d CCC: $40.75
Published on Web 02/08/2008

Scheme 1. Synthesis of the Imide-Substituted Catechols and their Pt^{II} Diimine Complexes[a]

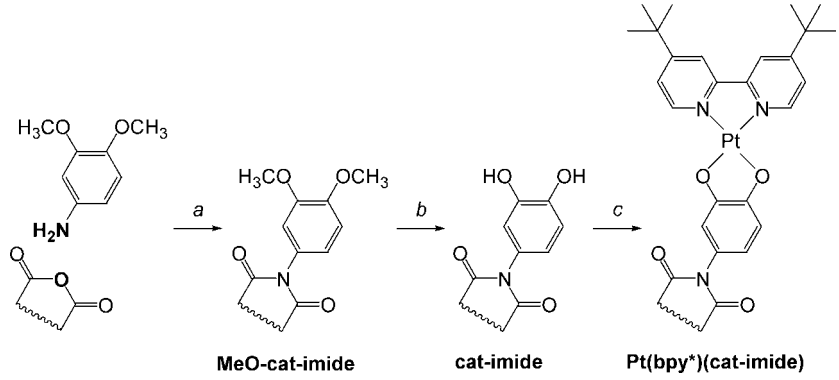

[a] Reaction conditions: (a) DMF, reflux, N_2, 24 hr; (b) BBr_3, CH_2Cl_2, RT, N_2, 24 hr; (c) Pt(bpy*)Cl_2, $NaHCO_3$, ethanol + DMF, 95°C, N_2, 24 hr.

Scheme 2. Synthesis of MeO-NAP-NDI[a]

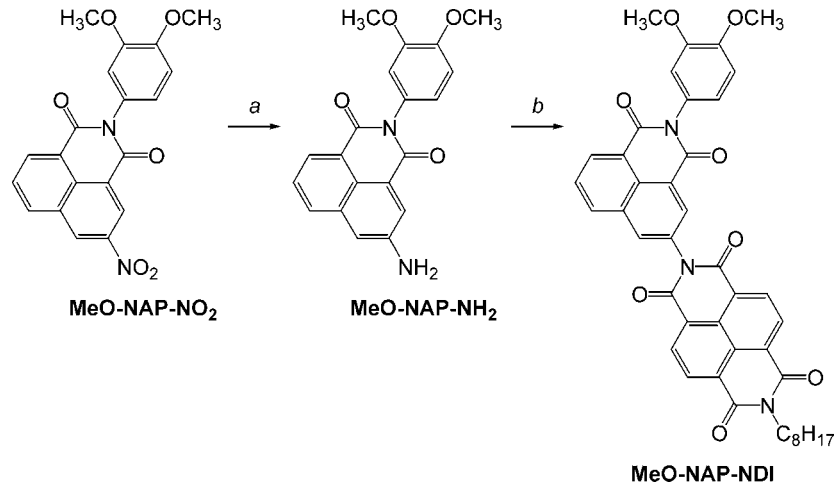

[a] Reaction conditions: (a) ammonium formate (excess), Pd/C, methanol, reflux, N_2, 6 hr; (b) DMF, reflux, N_2, 24 hr.

several (di)imide groups which have different reduction potentials and spectroscopic features of the corresponding radical anions seems to be an attractive option for a modular approach to generation of a cascade electron-transfer material.

The imides can be incorporated into metal complexes by an attachment to a suitable ligand, in which the imide group is bound to the ligand either directly or via a flexible linker, yielding different extents of electronic communication.[7–9] A combination of the imide, the binding ligand and the metal ion could provide chromophores with tuneable optical, electrochemical, and electrochromic properties. Yet the majority of imide-modified ligands reported are neutral pyridine derivatives, with only few examples of anionic ligands[10] being described.

Herein, we report the syntheses of anionic catechol ligands with imide groups attached directly to the 4-position of the catechol moiety. These ligands combine both strong electron-donor (catechol) and electron-acceptor (imide) functionalities. Catechol ligands have been used extensively in coordination chemistry of various metal ions,[11–16] although Pt^{II}–catecholate chemistry has been relatively under-explored.[13,17,18]

The attractive feature of catecholate ligands[19,20] is their facile and reversible oxidation to semiquinone and quinone, accompanied by dramatic changes in the light absorption properties across the visible region, which has been exploited in the preparation of many magnetic and electrochromic materials based on metal catecholates.[21]

(1) (a) Holtrup, F. O.; Müller, G. R. J.; Uebe, J.; Müllen, K. *Tetrahedron* **1997**, *53*, 6847. (b) Langhals, H.; Ismael, R.; Yuruk, O. *Tetrahedron* **2000**, *56*, 5435. (c) Katz, H. E.; Siegrist, T.; Schon, J. H.; Kloc, C.; Batlogg, B.; Lovinger, A. J.; Johnson, J. *ChemPhysChem* **2001**, 167. (d) Kolosov, D.; Adamovich, V.; Djurovich, P.; Thompson, M. E.; Adachi, C. *J. Am. Chem. Soc.* **2002**, *124*, 9945. (e) Wu, J.; Qu, J.; Tchebotareva, N.; Müllen, K. *Tetrahedron Lett.* **2005**, *46*, 1565. (f) Yukruk, F.; Dogan, A. L.; Canpinar, H.; Guc, D.; Akkaya, E. U. *Org. Lett.* **2005**, *7*, 2885. (g) Cao, H.; Chang, V.; Hernandez, R.; Heagy, M. D. *J. Org. Chem.* **2005**, *70*, 4929. (h) Xiao, Y.; Fu, M.; Qian, X.; Cui, J. *Tetrahedron Lett.* **2005**, *46*, 6289. (i) Wurthner, F.; Chen, Z.; Dehm, V.; Stepanenko, V. *Chem. Commun.* **2006**, 1188.

(2) Hayes, R. T.; Wasielewski, M. R.; Gosztola, D. *J. Am. Chem. Soc.* **2000**, *122*, 5563.

(3) Gosztola, D.; Niemczyk, M. P.; Svec, W.; Lukas, A. S.; Wasielewski, M. R. *J. Phys. Chem. A* **2000**, *104*, 6545.

(4) (a) Ferrere, S.; Zaban, A.; Gregg, B. A. *J. Phys. Chem. B* **1997**, *101*, 4490. (b) Tomizaki, K.-y.; Thamyongkit, P.; Loewe, R. S.; Lindsey, J. S. *Tetrahedron* **2003**, *59*, 1191. (c) Takenaka, S.; Uto, Y.; Saita, H.; Yokoyama, M.; Kondo, H.; Wilson, W. D. *Chem. Commun.* **1998**, 1111. (d) Saito, I.; Takayama, M.; Kawanishi, S. *J. Am. Chem. Soc.* **1995**, *117*, 5590. (e) Qian, X.; Li, Y.; Xu, Y.; Liu, Y.; Qu, B. *Bioorg. Med. Chem. Lett.* **2004**, *14*, 2665.

(5) Leedy, D. W.; Muck, D. L. *J. Am. Chem. Soc.* **1971**, *93*, 4264.

(6) Andric, G.; Boas, J. F.; Bond, A. M.; Fallon, G. D.; Ghiggino, K. P.; Hogan, C. F.; Hutchison, J. A.; Lee, M. A.-P.; Langford, S. J.; Pilbrow, J. R.; Troup, G. J.; Woodward, C. P. *Aust. J. Chem.* **2004**, *57*, 1011.

(7) Flamigni, L.; Baranoff, E.; Collin, J.-P.; Sauvage, J.-P. *Chem.—Eur. J.* **2006**, *12*, 6592.

Catechol and imide groups clearly complement one another with respect to the range of the easily accessible redox states, each possessing characteristic intense absorptions across the UV–vis−NIR spectral region.

The coordination properties of these ligands have been exploited in the synthesis of the corresponding Pt^{II} diimine complexes. The electronic structure, intramolecular electronic communication, and rich electrochemistry and electrochromism of this class of chromophores are discussed in detail.

Results and Discussion

Syntheses[22]. A simple two-step reaction sequence was used to prepare new catechol ligands, cat-imide (Scheme 1 and 2). In the first step, 4-aminoveratrole (methyl-ether-protected catechol) was reacted with an appropriate aromatic acid anhydride in DMF at reflux to give the corresponding imide (MeO-cat-imide). The key intermediate in the synthesis of MeO-NDI and MeO-NAP-NDI imides is *N*-octyl-1,4,5,8-naphthalenetetracarboxylic monoanhydride; the improved procedure for its synthesis is described in the Experimental Section.

In the second step, the catechol group was deprotected using BBr_3 in CH_2Cl_2 to give the ligand, cat-imide. Both reactions proceeded with high yield and gave the product that often did not require further purification. Four new catechol ligands and one bridging bis-catechol ligand were prepared in this way (Scheme 3). It should be noted that our attempts to prepare catechol ligands by a direct reaction of acid anhydride with 4-aminocatechol (DMF, reflux) have failed.

The key step in the synthesis of catechol NAP-NDI was the reduction of the nitro group to an amino group in 3-nitro-1,8-naphthalic imide (MeO-NAP-NO_2) using ammonium formate and Pd/C catalyst[23] in methanol at reflux.

The reaction of catechols with Pt(bpy*)Cl_2 (bpy* = 4,4′-di*tert*-butyl-2,2′-bipyridine) in hot ethanol−DMF in the presence of $NaHCO_3$, as a base, afforded four new catecholate complexes, Pt(bpy*)(cat-imide). All complexes were purified by column chromatography. The reaction of bridging bis-catechol ligand BTC with Pt(bpy*)Cl_2 led to a product that was not sufficiently soluble for further purification and, therefore, was not studied any further.

All new compounds were identified by EI mass-spectrometry, elemental analysis, and ^{1}H NMR spectroscopy.

(8) (a) Hossain, Md. D.; Haga, M.-a.; Monjushiro, H.; Gholamkhass, B.; Nozaki, K.; Ohno, T. *Chem. Lett.* **1997**, 573. (b) Dixon, D. W.; Thornton, N. B.; Steullet, V.; Netzel, T. *Inorg. Chem.* **1999**, *38*, 5526. (c) Tyson, D. S.; Luman, C. R.; Zhou, X.; Castellano, F. N. *Inorg. Chem.* **2001**, *40*, 4063. (d) Johansson, O.; Borgstrom, M.; Lomoth, R.; Palmblad, M.; Bergquist, J.; Hammarstrom, L.; Sun, L.; Akermark, B. *Inorg. Chem.* **2003**, *42*, 2908. (e) Kirmaier, C.; Hindin, E.; Schwartz, J. K.; Sazanovich, I. V.; Diers, J. R.; Muthukumaran, K.; Taniguchi, M.; Bocian, D. F.; Lindsey, J. S.; Holten, D *J. Phys. Chem. B* **2003**, *107*, 3443–3454.

(9) (a) Sautter, A.; Kaletas, B. K.; Schmid, D. G.; Dobrawa, R.; Zimine, M.; Jung, G.; van Stokkum, I. H. M.; De Cola, L.; Williams, R. M.; Wurthner, F. *J. Am. Chem. Soc.* **2005**, *127*, 6719. (b) Addicott, C.; Oesterling, I.; Yamamoto, T.; Mullen, K.; Stang, P. J. *J. Org. Chem.* **2005**, *70*, 797. (c) Du, P.; Li, C.; Li, S.; Zhu, W.; Tian, H. *Synth. Met.* **2003**, *137*, 1131. (d) Lu, X.-Q.; Jiang, J.-J.; zur Loye, H.-C.; Kang, B.-S.; Su, C.-Y. *Inorg. Chem.* **2005**, *44*, 1810. (e) Reger, D. L.; Elgin, J. D.; Semeniuc, R. F.; Pellechia, P. J.; Smith, M. D. *Chem. Commun.* **2005**, 4068. (f) Wang, J.; Xiao, Y.; Zhang, Z.; Qian, X.; Yang, Y.; Xu, Q *J. Mater. Chem.* **2005**, *15*, 2836. (g) Houghton, M. A.; Bilyk, A.; Harding, M. M.; Turner, P.; Hambley, T. W. *J. Chem. Soc., Dalton Trans.* **1997**, 2725. (h) Licchelli, M.; Biroli, A. O.; Poggi, A. *Org. Lett.* **2006**, *8*, 915.

(10) (a) Xu, Z.; Qian, X.; Cui, J. *Org. Lett.* **2005**, *7*, 3029. (b) Fan, L.; Zhu, W.; Li, J.; Tian, H. *Synth. Met.* **2004**, *145*, 203. (c) McGale, E. M.; Murray, R. E.; McAdam, C. J.; Morgan, J. L.; Robinson, B. H.; Simpson, J. *Inorg. Chim. Acta* **2003**, *352*, 129. (d) McAdam, C. J.; Manning, A. R.; Robinson, B. H.; Simpson, J. *Inorg. Chim. Acta* **2005**, *358*, 1673. (e) Yoshida, N.; Ishizuka, T.; Yofu, K.; Murakami, M.; Miyasaka, H.; Okada, T.; Nagata, Y.; Itaya, A.; Cho, H. S.; Kim, D.; Osuka, A. *Chem.−Eur. J.* **2003**, *9*, 2854. (f) Li, Y.; Wang, N.; Gan, H.; Liu, H.; Li, H.; Li, Y.; He, X.; Huang, C.; Cui, S.; Wang, S.; Zhu, D. *J. Org. Chem.* **2005**, *70*, 9686. (g) Weissman, H.; Shirman, E.; Ben-Moshe, T.; Cohen, R.; Leitus, G.; Shimon, L. J. W.; Rybtchinski, B. *Inorg. Chem.* **2007**, *46*, 4790.

(11) Girgis, A. Y.; Sohn, Y. S.; Balch, A. L. *Inorg. Chem.* **1975**, *14*, 2327.

(12) Kaim, W.; Wanner, M.; Knodler, A.; Zalis, S. *Inorg. Chim. Acta* **2002**, *337*, 163.

(13) Ghosh, P.; Begum, A.; Herebian, D.; Bothe, E.; Hildenbrand, K.; Weyhermuller, T.; Wieghardt, K. *Angew. Chem., Int. Ed.* **2003**, *42*, 563.

(14) (a) Peacock, A. F. A.; Batey, H. D.; Raendler, C.; Whitwood, A. C.; Perutz, R. N.; Duhme-Klair, A.-K. *Angew. Chem., Int. Ed.* **2005**, *44*, 1712. (b) Kriegisch, V.; Lambert, C. *Eur. J. Inorg. Chem.* **2005**, 4509. (c) Takemoto, S.; Ogura, S.-I.; Kamikawa, K.; Matsuzaka, H. *Inorg. Chim. Acta* **2006**, *359*, 912.

(15) (a) Base, K.; Tierney, M. T.; Fort, A.; Muller, J.; Grinstaff, M. W. *Inorg. Chem.* **1999**, *38*, 287. (b) Rauth, G. K.; Pal, S.; Das, D.; Sinha, C.; Slawin, A. M. Z.; Woollins, J. D. *Polyhedron* **2001**, *20*, 363. (c) Pal, S.; Das, D.; Sinha, C.; Kennard, C. H. L. *Inorg. Chim. Acta* **2001**, *313*, 21. (d) Kinder, J. D.; Youngs, W. J. *Organometallics* **1996**, *15*, 460. (e) Daldy, J. A.; Fawcett, J.; Henderson, W.; Kemmitt, R. D. W.; Russell, D. R. *J. Chem. Soc., Dalton Trans.* **1994**, 3383. (f) Bohle, D. S.; Stasko, D. *Chem. Commun.* **1998**, *567*. (g) Casas, J. M.; Falvello, L. R.; Fornies, J.; Mansilla, G.; Martin, A. *Polyhedron* **1999**, *18*, 403. (h) Anbalagan, V.; Srivastava, T. S. *Polyhedron* **2004**, *23*, 3173.

(16) Hartl, F.; Barbaro, P.; Bell, I. M.; Clark, R. J. H.; Snoeck, T. L.; Vlcek, A *Inorg. Chim. Acta* **1996**, *252*, 157.

(17) Weinstein, J. A.; Tierney, M. T.; Davies, E. S.; Base, K.; Robeiro, A. A.; Grinstaff, M. W. *Inorg. Chem.* **2006**, *45*, 4544.

(18) (a) Paw, W.; Eisenberg, R. *Inorg. Chem.* **1997**, *36*, 2287. (b) Hill, P. L.; Lee, L. Y.; Younkin, T. R.; Orth, S. D.; McElwee-White, L. *Inorg. Chem.* **1997**, *36*, 5655. (c) Shukla, A. D.; Whittle, B.; Bajaj, H. C.; Das, A.; Ward, M. D. *Inorg. Chim. Acta* **1999**, *285*, 89. (d) Fujihara, T.; Okamura, R.; Wada, T.; Tanaka, K. *Dalton Trans.* **2003**, 3221. (e) Gandolfi, O.; Cais, M.; Dolcetti, G.; Ghedini, M.; Modiano, A. *Inorg. Chim. Acta* **1981**, *56*, 127. (f) Howell, B. A.; Rashidianfar, R.; Glass, J. R.; Hutchinson, B. J.; Johnson, D. A. *Inorg. Chim. Acta* **1988**, *142*, 181. (g) Apfelbaum, H. C.; Blum, J.; Mandelbaum-Shavit, F. *Inorg. Chim. Acta* **1991**, *186*, 243. (h) Hirani, B.; Li, J.; Djurovich, P. I.; Yousufuddin, M.; Oxgaard, J.; Persson, P.; Wilson, S. R.; Bau, R.; Goddard, W. A., III; Thompson, M. E. *Inorg. Chem.* **2007**, *46*, 3865.

(19) (a) Pierpont, C. G.; Buchanan, R. M. *Coord. Chem. Rev.* **1981**, *38*, 45. (b) Pierpont, C. G. *Coord. Chem. Rev.* **2001**, *219–221*, 415. (c) Dei, A.; Gatteschi, D.; Sangregorio, C.; Sorace, L. *Acc. Chem. Res.* **2004**, *37*, 827.

(20) (a) Caulder, D. L.; Raymond, K. N. *J. Chem. Soc., Dalton Trans.* **1999**, 1185. (b) Albrecht, M.; Janser, I.; Frohlich, R. *Chem. Commun.* **2005**, 157.

(21) (a) Haga, M.; Dodsworth, E. S.; Lever, A. B. P. *Inorg. Chem.* **1986**, *25*, 447. (b) Barthram, A. M.; Cleary, R. L.; Kowallick, R.; Ward, M. D. *Chem. Commun.* **1998**, 2695. (c) Shukla, A. D.; Ganguly, B.; Dave, P. C.; Samanta, A.; Das, A. *Chem. Commun.* **2002**, 2648. (d) Schwab, P. F. H.; Diegoli, S.; Biancardo, M.; Bignozzi, C. A. *Inorg. Chem.* **2003**, *42*, 6613.

(22) The following abbreviations are used: For a general reference to the new class of ligands and complexes, cat-imide and Pt(bpy*)(cat-imide) are used. For individual catechol ligands, PHT, NAP, NDI, NAP-NDI, and 3,5-cat are used. For individual complexes, Pt(bpy*)PHT, Pt(bpy*)NAP, Pt(bpy*)NDI, Pt(bpy*)NAP-NDI, and Pt(bpy*)(3,5-cat). The imide complexes are also referred to in the text as the PHT complex, NAP complex, etc.

(23) (a) Ram, S.; Ehrenkaufer, R. E. *Tetrahedron Lett.* **1984**, *25*, 3415. (b) Ram, S.; Ehrenkaufer, R. E. *Synthesis* **1988**, 91. (c) Gunnlaugsson, T.; Kruger, P. E.; Jensen, P.; Pfeffer, F. M.; Hussey, G. M *Tetrahedron Lett.* **2003**, *44*, 8909.

Scheme 3. New Catechol Ligands Prepared in the Study

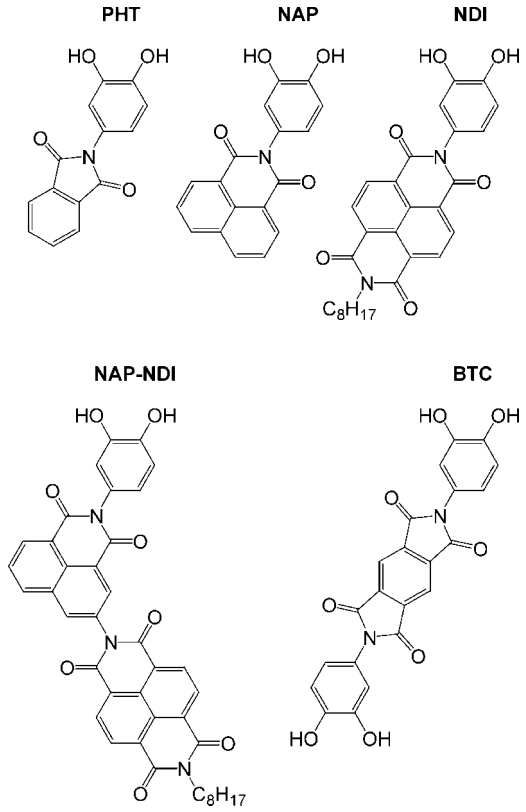

X-Ray Crystallography. Crystal structures of two Pt(bpy*)(cat-imide) complexes (cat-imide = PHT or NAP) are shown in Figures 1 and 2. The structural features are similar for both complexes.

The Pt^{II} center is in a distorted square planar coordination environment. The bpy* ligand is nearly planar. The dihedral angle between the two pyridyl rings of bpy* is 3.70° (PHT) and 1.73° (NAP). The catechol and imide groups are planar and are orthogonal to each other with dihedral angles of ~70°.

Both complexes form dimers in the solid state through Pt···Pt contacts of 3.208 (PHT) and 3.378 Å (NAP). These distances are remarkably short[24] considering that the Pt···Pt interaction is not supported by a bridging ligand. This Pt···Pt interaction might be facilitated by an aromatic $\pi-\pi$ interaction between the bpy* and the catechol units within a dimer (these ligands are positioned above each other but they are not parallel).

The Pt···Pt dimers are further packed in a columnlike structure. The interdimer interaction occurs through the aromatic $\pi-\pi$ stacking of bpy* ligands. The bpy* planes are parallel to each other with interplanar distances of 3.327 (PHT) and 3.390 Å (NAP) (the planes included all nonhydrogen atoms of bpy* apart from ^{t}Bu groups). The interdimer Pt···Pt distances are 4.979 (PHT) and 5.203 Å (NAP).

Absorption Spectroscopy. The UV–vis absorption spectra of the new ligands and their Pt^{II}(bpy*) complexes, recorded in CH_2Cl_2 at room temperature, are shown in Figure 3, and the main spectral features are summarized in Table 1.

(24) (a) Cini, R.; Fanizzi, F. P.; Intini, F. P.; Maresca, L.; Natile, G. *J. Am. Chem. Soc.* **1993**, *115*, 5123. (b) Novoa, J. J.; Aullon, G.; Alemany, P.; Alvarez, S. *J. Am. Chem. Soc.* **1995**, *117*, 7169. (c) Poater, A.; Moradell, S.; Pinilla, E.; Poater, J.; Sola, M.; Martinez, M. A.; Llobet, A. *Dalton Trans.* **2006**, 1188.

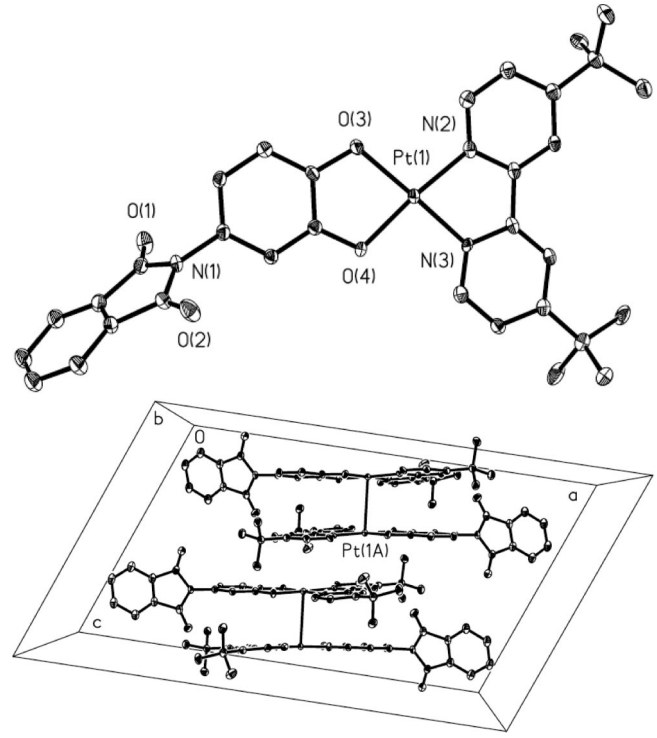

Figure 1. Molecular structure of Pt(bpy*)PHT (top-view) and columnlike packing of molecules (side-view) (50% probability ellipsoids, H atoms, and cocrystallized molecule of H_2O omitted). Selected bond lengths (Å): Pt(1)−N(3) = 1.973(5), Pt(1)−N(2) = 1.994(4), Pt(1)−O(4) = 1.998(4), Pt(1)−O(3) = 2.014(4), Pt(1)−Pt(1)#1 = 3.2084(4). Selected angles (deg): N(3)−Pt(1)−N(2)=80.34(19),O(4)−Pt(1)−O(3)=84.08(15),N(3)−Pt(1)−O(4) = 94.18(17), N(2)−Pt(1)−O(3) = 101.39(17), N(2)−Pt(1)−O(4) = 174.18(17), N(3)−Pt(1)−O(3) = 178.26(16). The dihedral angle between the planes defined by the N(2) Pt(1) N(3) and O(3) Pt(1) O(4) atoms is 1.99°.

The catecholate ligands were obtained as white or yellow solids. Their absorption spectra do not have bands at wavelengths longer than 400 nm (Figures 1S and 2S, Supporting Information).

The catecholate complexes, Pt(bpy*)(cat-imide), were obtained as deep-blue solids. Their absorption spectra feature a broad and structureless lowest-energy band, centered at ~530 nm, with an extinction coefficient of $\sim 6{\cdot}10^3\ M^{-1}\ cm^{-1}$ (Table 1). The lack of this absorption band either in the spectrum of Pt(bpy*)Cl_2 (Figure 3S) or in the spectra of the cat-imide ligand precursors suggest that this electronic transition is predominantly ligand-to-ligand charge transfer (LLCT) in nature. The energy and extinction coefficient of this absorption band are virtually identical for all Pt(bpy*)(cat-imide) complexes and for Pt(bpy*)(3,5-cat), and are very similar to those reported previously for catecholate-to-diimine charge transfer transition in other Pt^{II} diimine catecholate complexes.[13,17] Therefore this absorption band in Pt(bpy*)(cat-imide)s is attributed to the predominantly ligand-to-ligand charge transfer transition, from the catecholate group of the cat-imide ligand to bpy*. The energy of this LLCT absorption band is remarkably insensitive to the nature of the imide group, indicating a lack of electronic communication between the catecholate and the imide groups in solution, which is

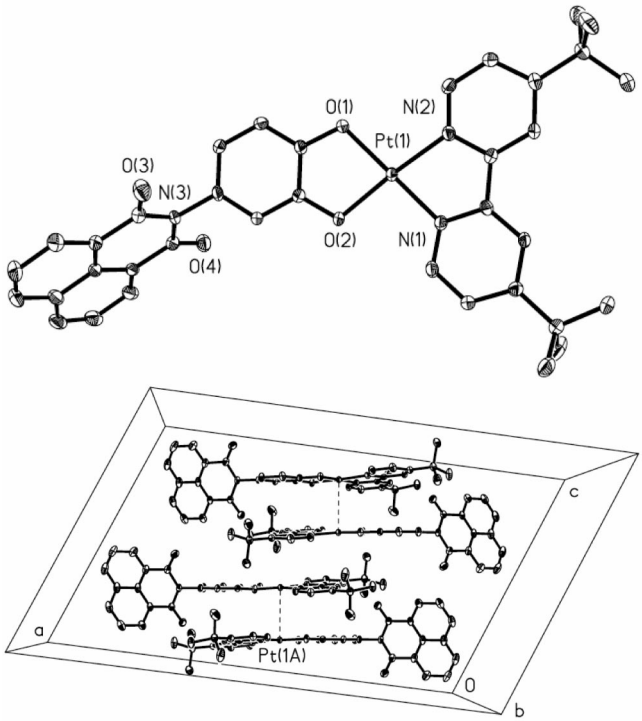

Figure 2. Molecular structure of Pt(bpy*)NAP (top-view) and columnlike packing of molecules (side-view) (50% probability ellipsoids, H atoms, and cocrystallized molecules of CH_3CN and H_2O omitted). Selected bond lengths (Å): Pt(1)−N(1) = 1.973(2), Pt(1)−N(2) = 2.001(2), Pt(1)−O(1) = 2.0122(17), Pt(1)−O(2) = 1.9904(17). Selected angles (deg): N(1)−Pt(1)−N(2) = 79.90(9), N(1)−Pt(1)−O(2) = 95.51(8), N(2)−Pt(1)−O(1) = 100.45(8), O(2)−Pt(1)−O(1) = 84.19(7), O(2)−Pt(1)−N(2) = 174.60(8), N(1)−Pt(1)−O(1) = 178.94(8). The dihedral angle between the planes defined by the N(1) Pt(1) N(2) and O(1) Pt(1) O(2) atoms is 3.14°.

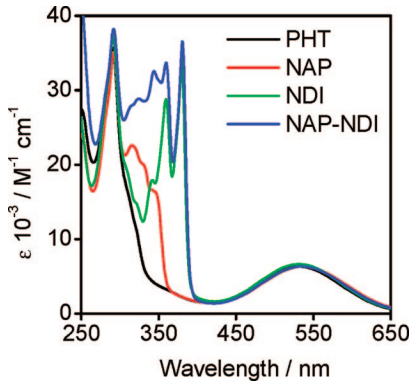

Figure 3. Absorption spectra of Pt(bpy*)(cat-imide) complexes in CH_2Cl_2 at ambient temperature.

consistent with the nearly orthogonal arrangements of these two groups in the solid state (Figures 1 and 2). The observations summarized above also rule out an intraligand catecholate-to-imide charge transfer assignment of the lowest-absorption band. The relatively high extinction coefficient of the charge-transfer transition is caused by the Pt contribution into the orbitals involved, as revealed by EPR spectroscopy of the complexes in various redox states (vide infra).

The LLCT absorption band in all Pt(bpy*)(cat-imide) complexes is termochromic, shifting to higher energies upon cooling of CH_2Cl_2 solutions from 298 to 253 K (see Table 4 for details).

Table 1. Absorption Spectra of the Catechols in THF and of the Complexes Pt(bpy*)Cl_2, Pt(bpy*)(3,5-cat), and Pt(bpy*)(cat-imide) in CH_2Cl_2

compound	λ_{max}/nm (10^{-3} ϵ/M^{-1} cm^{-1})
	ligands
PHT	281 (7.7, sh)
BTC	330 (5.2, sh), 292 (19)
NAP	340 (12), 330 (14), 287 (5.5)
NDI	378 (26), 358 (22), 341 (14), 287 (7.1)
NAP-NDI	379 (31), 358 (28), 343 (28), 289 (10)
	complexes
Pt(bpy*)Cl_2	389 (4.1), 322 (8.4), 311 (7.8), 281 (26), 257 (17)
Pt(bpy*)(3,5-cat)	577 (5.7), 377 (2.5), 297 (29), 249 (20)
PHT	532 (6.4), 291 (36)
NAP	535 (6.3), 341 (17), 330 (20), 316 (23), 292 (35)
NDI	532 (6.7), 380 (34), 359 (29), 342 (18), 291 (37)
NAP-NDI	535 (6.3), 381 (37), 360 (34), 344 (33), 323 (29), 292 (38)

Table 2. Absorption Spectra of the Pt(bpy*)NDI Complex in Different Solvents

solvent	solvent parameter[a]	λ_{max}/nm (10^{-3} ϵ/M^{-1} cm^{-1})
THF	0.494	576 (6.8), 378 (31), 358 (27), 341 (17), 296 (38)
$CHCl_3$	0.610	552 (6.4), 380 (34), 360 (28), 342 (17), 294 (38)
CH_2Cl_2	0.765	532 (6.7), 380 (34), 359 (29), 342 (18), 291 (37)
acetone	0.797	532 (6.8), 376 (32), 357 (28), 339 (18)
DMF	0.901	523 (6.6), 380 (28), 360 (25), 343 (17), 292 (35)
CH_3CN	1.000	506 (6.8), 376 (33), 357 (28), 340 (18), 287 (34)

[a] The solvent polarity parameter data were taken from ref 27.

The absorption spectra of the cat-imide ligands and their Pt^{II} complexes in the region 250–400 nm were determined by the imide group. The characteristic intense structured absorption bands of 1,8-naphthalimide or 1,4,5,8-naphthalenediimide chromophores[25,26] were observed in the spectra of the NAP, NDI, and NAP-NDI catechols and their Pt^{II} complexes.

Solvatochromism. The absorption properties of Pt(bpy*)NDI complex in solvents of different polarity are summarized in Table 2. The lowest absorption band shows negative solvatochromism, that is, the absorption maximum is red-shifted with the decrease of solvent polarity, from 506 nm in CH_3CN to 576 nm in THF. This feature is consistent with the inversion of the dipole moment upon formation of catecholate-to-diimine CT excited state. A linear correlation has been observed between the energy of the lowest-absorption band and the solvent polarity parameter value based on the energy of the charge-transfer-to-diimine transition in Pt(bpy*)(toluene-3,4-dithiolate).[27] The slope of the linear correlation between the absorption energy and this solvent polarity parameter gives the value for the solvatochromic shift of 4430 cm^{-1} (0.55 eV) (Figure 4S in the Supporting Information), which falls within the range reported previously for LLCT transitions in Pt^{II} diimine catecholate complexes.

The 1,4,5,8-naphthalenediimide-centered absorption bands (378, 358 and 341 nm)[25] in the Pt(bpy*)NDI complex were

(25) (a) Barros, T. C.; Brochsztain, S.; Toscano, V. G.; Filho, P. B.; Politi, M. J. *J. Photochem. Photobiol. A: Chem.* **1997**, *111*, 97. (b) Alp, S.; Erten, S.; Karapire, C.; Koz, B.; Doroshenko, A. O.; Icli, S. *J. Photochem. Photobiol. A: Chem.* **2000**, *135*, 103. (c) Prezhdo, O. V.; Uspenskii, B. V.; Prezhdo, V. V.; Boszczyk, W.; Distanov, V. B. *Dyes Pigm.* **2007**, *72*, 42.
(26) Rogers, J. E.; Kelly, L. A. *J. Am. Chem. Soc.* **1999**, *121*, 3854.
(27) Cummings, S. D.; Eisenberg, R. *J. Am. Chem. Soc.* **1996**, *118*, 1949.

Table 3. Electrochemical Data (in mV vs Fc^+/Fc) for the 1 mM Solutions of Pt(bpy*)(cat-imide) Complexes in CH_2Cl_2 Containing 0.4 M $[NBu_4][PF_6]$ and in DMF Containing 0.2 M $[NBu_4][PF_6]$[a]

complex	solvent	reduction	oxidation[c]
PHT	CH_2Cl_2	−1990 (80), *pht*; −1780 (80), *bpy**	130 (110)
	DMF	−1960 (70), *pht*; −1790 (70), *bpy**	130 (70)
NAP	CH_2Cl_2	*−1840*, *−1800*,[b] *nap/bpy**	*70*, *190*[b]
	DMF	−1800 (100), *nap/bpy**	110 (90)
NDI	CH_2Cl_2	−1850 (80), *bpy**; −1480 (80), *ndi*; −1030 (80) *ndi*	*130*, *200*[b]
	DMF	−1820 (70), *bpy**; −1520 (70), *ndi*; −1010 (70), *ndi*	140 (90)
NAP-NDI	CH_2Cl_2	*−1880*, *−1800*[b] *nap/bpy**; −1390 (70), *ndi*; −950 (80), *ndi*	*110*, *200*[b]
	DMF	*−1880*, *−1800*[b] *nap/bpy**; −1400 (70), *ndi*; −930 (70), *ndi*	120 (80)
3,5-cat	CH_2Cl_2	−1820 (80)	−180 (80)
	DMF	−1820 (70)	−100 (70)
$Pt(bpy^*)Cl_2$	DMF	−1700 (70)	

[a] The following abbreviations were used: pht = phthalimide group, nap = 1,8-naphthalimide group, and ndi = 1,4,5,8-naphthalenediimide group. The anodic/cathodic peak separation is given in brackets where applicable. The anodic/cathodic peak separation for the standard, Fc^+/Fc couple, was 70 mV in all experiments. The oxidation process is localized on the catecholate moiety of the cat-imide ligand, and the suggested assignment of the localization of the reduction processes is indicated in italic. [b] Cyclic voltammetry gave closely overlapped processes that were resolved by square wave voltammetry. [c] All Pt(bpy*)(cat-imide) complexes exhibit another oxidation process at ca. 1 V.

not solvatochromic, as could be anticipated for ligand-centered transitions. The extinction coefficients of both the LLCT and the imide-centered bands were not particularly sensitive to the solvent polarity.

Luminescence and Transient Absorption Spectroscopy. Similar to the other Pt^{II} catecholate complexes,[17] Pt(bpy*)(cat-imide) complexes do not show luminescence in degassed CH_2Cl_2 solutions at room temperature.

Nanosecond flash-photolysis of Pt(bpy*)NDI in dry degassed CH_2Cl_2 under excitation into LLCT band (532 nm) has not revealed the formation of any transient species with a lifetime >20 ns in the spectral range of 400–800 nm.

Electrochemistry. The Pt(bpy*)(cat-imide) complexes show a series of redox processes in the potential window between 1.0 and −2.5 V (all potentials are quoted vs Fc^+/Fc). The cyclic voltamograms recorded in CH_2Cl_2 solution are shown in Figure 4, and the redox potentials are summarized in Table 3. Data for the model compound Pt(bpy*)(3,5-cat), where 3,5-cat is 3,5-di-*tert*-butyl-catecholate, are also given for comparison. Data recorded in DMF are summarized in Table 3 and Figure 6S.

Cyclic Voltammetry: Reduction. The Pt(bpy*)(cat-imide) complexes show several reductions in the range from −0.95 to −1.99 V that could be located either on the bpy* or the imide group.[28] The assignments of these reduction processes were based on UV−vis spectroelectrochemical studies and EPR spectroscopy.

Reduction of Pt(bpy*)PHT appeared as two partially overlapped processes. Results of EPR spectroscopy allowed us to assign the first one-electron reduction at −1.78 V to bpy* and the second reduction at −1.99 V to the phthalimide group. The reduction of the Pt(bpy*)NAP was observed as two overlapped one-electron processes at −1.82 V, which are likely to be located on the bpy* and 1,8-naphthalimide moieties but were not assigned specifically. For Pt(bpy*)NDI, the first and the second one-electron reductions, at −1.03 and −1.48 V, respectively, were located on the 1,4,5,8-naphthalenediimide group, while the third reduction at −1.85 V was centered on the bpy* ligand. The first and second one-electron reduction processes of the Pt(bpy*)NAP-NDI, at −0.95 and −1.39 V, respectively, were located on the 1,4,5,8-naphthalenediimide, while the third and the fourth closely overlapping reduction processes (−1.80 and −1.88 V) are likely to be centered on 1,8-naphthalimide and bpy*, but the sequence was not determined. These data demonstrate that the 1,4,5,8-naphthalenedimiide substituted 1,8-naphthalimide group in NAP-NDI ligand can undergo three reduction processes in a stepwise fashion.

Cyclic Voltammetry: Oxidation. The first oxidation process observed in CH_2Cl_2 solution between 0.07 and 0.20 V is chemically reversible for all complexes, as shown by UV−vis spectroelectrochemistry. Comparison with the oxidation potentials reported previously for the Pt^{II} catecholates[13,17,18a] and Pt(bpy*)(3,5-cat), as well as spectroelectrochemical studies discussed below allowed for an assignment of the first process to an oxidation of the coordinated catechol to semiquinone. The subsequent oxidation, at $E_p^a \approx 1.0$ V was not investigated further but is likely to be associated with the semiquinone to quinone oxidation.

The overall first oxidation process amounts to a net transfer of *one electron*, as confirmed by coulometry for all Pt(bpy*)(cat-imide) complexes. The scan rate dependence recorded for the oxidation process in the range 20–300 mV s^{-1}, reveals no variation in the wave shape, and any variation in observed peak positions was consistent entirely with the variation in peak position observed for Fc^{*+}/Fc^* used as the internal standard. However, the current response for the oxidation process is concentration dependent (Figure 4, inset), as revealed by the studies of NDI and PHT (Figure 5S) complexes. At low concentrations (e.g., ∼0.1 mM for NDI complex), the electron transfer resembled that of a simple diffusion controlled process. At higher concentrations, the oxidation appears as two successive, closely overlapping electron transfer processes in both the first and second half-cycles of the cyclic voltammetry. Such perturbation of the CV profile becomes more pronounced with an increase of the size of the imide group: Figure 4 demonstrates that at an intermediate, 1 mM, concentrations, the CV of the oxidation of the PHT complex still appears as a single wave, albeit with a very large separation between anodic and cathodic peaks, while for NAP, NDI, and NAP-NDI complexes, it is

(28) The first reduction potential of imide group follows the trend phthalimide, ∼−1.9 V < 1,8-naphthalimide, ∼−1.8 V < 1,4,5,8-naphthalenediimide, ∼−1.0 V. The 1,4,5,8-naphthalenediimide undergoes two consecutive one-electron reductions with a difference in potential between those of ∼0.4 V. (See refs 26 and 3.)

Table 4. (a) Absorption Spectra of the Neutral, Oxidized, and Reduced Forms of the 0.5 mM Solutions of Pt(bpy*)(cat-imide) Complexes in CH_2Cl_2 Containing 0.4 M $[NBu_4][PF_6]$[a] and (b) Absorption Spectra of the Neutral and Reduced Forms of the Pt(bpy*)(cat-imide) and $Pt(bpy^*)Cl_2$ Complexes in DMF Containing 0.2 M $[NBu_4][PF_6]$ Obtained from 0.5 mM Solutions at 253 K

complex	λ_{max}/nm (10^{-3} ϵ/M^{-1} cm^{-1})
	a
PHT^{+1}	313 (23), 470 (10), 576 (5)
PHT^{0}[b]	288 (38), 509 (7)
NAP^{+1}	234 (93), 315 (26), 341 (30), 354 (25), 463 (8), 576 (4), 620 (4)
NAP^{0}	232 (92), 289 (41), 320 (28), 334 (25), 350 (21), 514 (8)
NAP^{-2}	231 (73), 273 (46), 298 (34), 359 (28), 422 (41), 492 (18), 739 (5), 815 (8)
NDI^{+1}	237 (78), 303 (21), 313 (23), 344 (23), 361 (34), 382 (41), 456 (8), 581 (4), 618 (4)
NDI^{0}	289 (40), 306 (23), 343 (21), 360 (34), 381 (42), 509 (8)
NDI^{-1}	273 (47), 291 (41), 377 (5), 401 (5), 479 (46), 592 (12), 611 (17), 680 (5), 753 (9)
NDI^{-2}[b]	236 (70), 242 (70), 293 (40), 400 (37), 423 (55), 515 (11), 552 (21), 600 (29)
$NAP\text{-}NDI^{+1}$	237 (125), 315 (31), 344 (42), 360 (49), 382 (49), 462 (8), 580 (4), 621 (4)
$NAP\text{-}NDI^{0}$	237 (123), 289 (42), 321 (33), 345 (38), 353 (37), 361 (41), 382 (46), 512 (7)
$NAP\text{-}NDI^{-1}$	271 (54), 290 (39), 320 (28), 332 (25), 403 (5), 479 (49), 589 (10), 609 (15), 689 (4), 764 (7)
$NAP\text{-}NDI^{-2}$[b]	245 (98), 289 (43), 310 (25), 338 (22), 400 (37), 423 (52), 521 (11), 559 (15), 608 (18)
$(3,5\text{-cat})^{+1}$	247 (32), 302 (15), 312 (15), 463 (9), 585 (4)
$(3,5\text{-cat})^{0}$ [b]	296 (32), 373 (3), 568 (6)
	b
PHT^{0}	290 (39), 511 (8)
PHT^{-1}	277 (29), 300 (27), 359 (24), 485 (12), 516 (15), 800 (2)
PHT^{-2}	310 (34), 362 (29), 442 (12), 487 (12), 520 (15), 815 (3)
NDI^{0}	291 (38), 344 (18), 360 (27), 381 (31), 517 (7)
NDI^{-1}	292 (34), 344 (7), 373 (5), 397 (5), 474 (41), 590 (10), 607 (14), 685 (4), 761 (7)
NDI^{-2}	295 (34), 378 (17), 398 (38), 422 (62), 480 (6), 515 (10), 555 (19), 603 (26)
NDI^{-3}	311 (24), 362 (26), 376 (21), 398 (40), 422 (66), 485 (12), 519 (16), 554 (17), 602 (23), 796 (1)
$(3,5\text{-cat})^{+1}$	305 (16), 315 (17), 465 (8), 601 (4)
$(3,5\text{-cat})^{0}$	297 (33), 372 (3), 566 (6)
$(3,5\text{-cat})^{-1}$	278 (18), 308 (22), 364 (21), 489 (10), 523 (13), 796 (2)
$[Pt(bpy^*)Cl_2]^{0}$	279 (27), 311 (10), 323 (12), 380 (5)
$[Pt(bpy^*)Cl_2]^{-}$	357 (17), 416 (8), 436 (7), 468 (8), 503 (12), 778 (2)

[a] The data were obtained from the spectroelectrochemistry experiments at 253 K. The reduction of the NAP-NDI complex was carried out at 273 K. It is noted that addition of $[NBu_4][PF_6]$ shifts the position of the LLCT absorption band in neutral complexes to higher energies (e.g., to 524 nm from 532 nm for Pt(bpy*)NDI). The LLCT absorption band also shifts to higher energies as the temperature of the solution decreases from 298 to 253 K (e.g., by 560 cm^{-1} for Pt(bpy*)NDI). [b] Subsequent reduction(s) not reversible in CH_2Cl_2.

already clearly split into two consecutive processes.

A possible explanation of these observations might relate to an aggregation of the electrochemically generated $[Pt(bpy^*)(cat\text{-}imide)]^{+\bullet}$ species in the diffusion layer under the conditions of cyclic voltammetry experiment, especially taking into account that aggregation of Pt^{II} complexes is a well-documented phenomenon.[29]

Therefore, an oxidation pathway involving the formation of $[M] + [M]^{+\bullet} \leftrightarrow [MM]^{+\bullet}$dimer species is proposed for

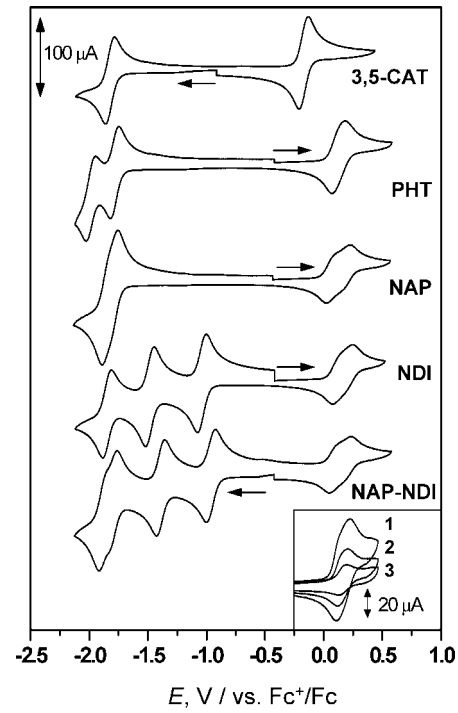

Figure 4. Cyclic voltamograms of 1 mM Pt(bpy*)(cat-imide) complexes in CH_2Cl_2 containing 0.4 M $[NBu_4][PF_6]$. Inset shows the change in the shape of the CV of the oxidation process of NDI complex at 0.51 (1), 0.26 (2), and 0.09 (3) mM. Scan rate = 100 mV/s.

CH_2Cl_2, where M = Pt(bpy*)(cat-imide). This monocation dimer $[MM]^{+\bullet}$ then undergoes a second electron transfer at potentials slightly more positive than that of the oxidation of [M], forming $[MM]^{2+}$.

It shall be noted that a similar concentration dependence of the CV profile for the oxidation process has been observed in DMF (Figure 6S). Arguably, much higher concentrations are required for the effect to become as pronounced in DMF as in CH_2Cl_2, which could, in principle, be attributed to a better solubilization of the complexes in DMF. However, this phenomenon could not be investigated in detail because of the chemical instability of the oxidized product in DMF.

The influence of the complex concentration on the observed behavior in the CV of the oxidation process strongly supports the dimerization hypothesis. This hypothesis was tested further by UV−vis and EPR spectroelectrochemistry.

UV−vis Spectroelectrochemistry. The nature of the frontier orbitals, the chemical reversibility of the redox processes, and the electrochromic properties of all the Pt(bpy*)(cat-imide) complexes were investigated by UV−vis spectroelectrochemistry at 253 K in CH_2Cl_2 solution (~0.5 mM). For selected compounds, reduction processes have also been investigated in DMF. Selected spectra are presented in Figures 5 and 6, and the absorption data for all redox forms

(29) (a) Houlding, V. H.; Miskowski, V. M *Coord. Chem. Rev.* **1991**, *111*, 145. (b) Connick, W. B.; Henling; L. M.; Marsh, R. E.; Gray, H. B *Inorg. Chem.* **1996**, *35*, 6261. (c) Siemeling, U.; Bausch, K.; Fink, H.; Bruhn, C.; Baldus, M.; Angerstein, B.; Plessow, R.; Brockhinke, A. *Dalton Trans.* **2005**, 2365. (d) Xiang, H.-F.; Chan, S.-C.; Wu, K. K.-Y.; Che, C.-M.; Lai, P. T *Chem. Commun.* **2005**, 1408. (e) Hissler, M.; McGarrah, J. E.; Connick, W. B.; Geiger, D. K.; Cummings, S. D.; Eisenberg, R *Coord. Chem. Rev.* **2000**, *208*, 115. (f) Yam, V.W.-W.; Wong, K. M.-C.; Zhu, N *J. Am. Chem. Soc.* **2002**, *124*, 6506.

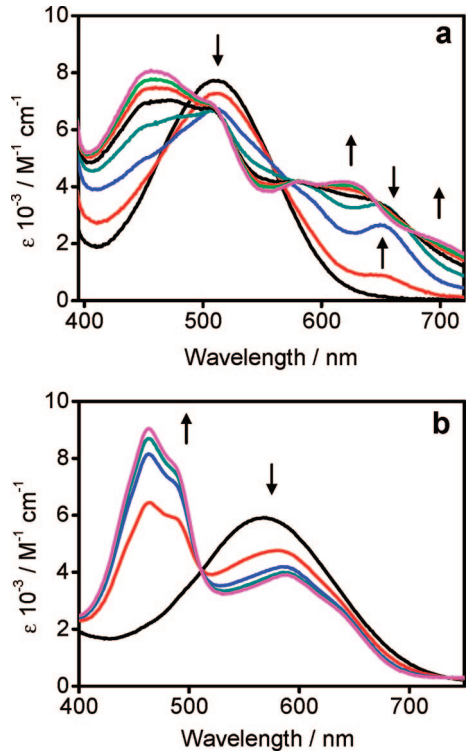

Figure 5. (a) Changes in the absorption spectra in the course of one-electron oxidation of 0.5 mM Pt(bpy*)NDI in CH_2Cl_2 containing 0.4 M $[NBu_4][PF_6]$ at 253 K. (b) Changes in the absorption spectra in the course of one-electron oxidation of 0.5 mM Pt(bpy*)(3,5-cat) in CH_2Cl_2 containing 0.4 M $[NBu_4][PF_6]$ at 253 K, which proceeds through isosbestic points, are shown for comparison.

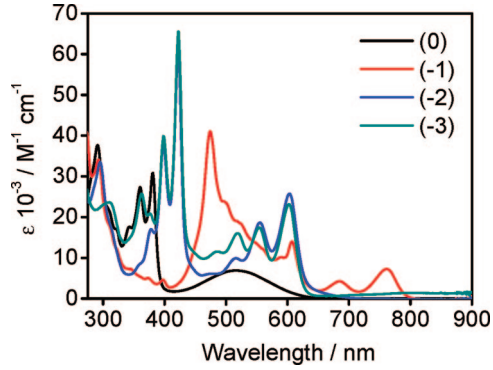

Figure 6. Absorption spectra of the neutral and one-/two-/three-electron-reduced forms of the complex Pt(bpy*)(NDI) in DMF containing 0.2 M $[NBu_4][PF_6]$ at 253 K obtained from the spectroelectrochemical experiments performed on 0.5 mM solution. The first two reduction processes were centred on the 1,4,5,8-naphthalenediimide group, and the third reduction was centered on the bpy* ligand.

are summarized in Table 4. Additional UV−vis spectroelectrochemical data are presented in Figures 7S−12S in the Supporting Information.

UV−vis Spectroelectrochemistry: Oxidation. The first oxidation process was chemically reversible for all Pt(bpy*)(cat-imide) complexes in CH_2Cl_2 at 253 K. The oxidation was accompanied by a depletion of the LLCT absorption band (506 nm at 253 K) and the formation of several new bands in the visible spectral region with maxima in the range of 456–470 and 580–621 nm. These bands can be assigned to absorption of a semiquinone radical cation coordinated to Pt^{II} by comparison with the spectroelectrochemical data reported for Pt(4,7-diphenyl-1,10-phenanthroline)(3,5-cat)[17] and for the model compound, Pt(bpy*)(3,5-cat).

Of particular interest was the progress of the oxidation that generated the final spectrum of the cationic species (Figures 5 and 12S). Oxidation of the model Pt(bpy*)(3,5-cat) compound progressed through a series of isosbestic points, indicating a $[M] \rightarrow [M]^{+\bullet}$ process in the absence of any long-lived intermediates or transition states (Figure 5b). In contrast, oxidation of Pt(bpy*)(cat-imide) exhibited a distinctly nonisosbestic behavior (Figure 5a). At early times during the electrolysis a band at ca. 650 nm was developed, which was depleted as electrolysis progressed and was not distinct in the final spectrum. Since the oxidation process could be reversed exactly on the spectroelectrochemical time scale, such behavior was attributed to generation of intermediate species during oxidation.

The spectroelectrochemical data thus correlate well with the proposed mechanism for oxidation from cyclic voltammetry: the absorption band at 650 nm could be a fingerprint of an intermediate dimeric species proposed above.

The formation and depletion of the 650 nm band in the course of the electrolysis, and the fact that the spectrum of the fully oxidized product is characteristic of $[M]^{+\bullet}$, suggests that the electrolysis proceeds via intermediate $[MM]^{+\bullet}$ species, while $[MM]^{2+}$ species are unstable and once formed, dissociate to give a monomer $[M]^{+\bullet}$. Such a hypothesis is consistent with results from EPR spectroscopy in fluid solution at room temperature, where the same EPR active species were observed at the 50% and 100% oxidation levels (vide infra).

The UV−vis spectroelectrochemical data in DMF can not be analyzed reliably because of the slight chemical irreversibility of the oxidation process, which is demonstrated by the lack of isosbestic points in the UV/vis spectra in the course of spectroelectrochemical oxidation and, more importantly, by the slight but distinct change of the spectral profile upon rereduction of the oxidized product if compared to the absorption spectrum of the initial neutral species (Figure 7S).

UV−vis Spectroelectrochemistry: Reduction. The reduction of the Pt(bpy*)NAP complex was accompanied by the disappearance of the absorption bands of 1,8-naphthalimide chromophore at 350 and 334 nm and the concomitant formation of the new absorption bands with maxima at 815, 739, 492, 422, and 273 nm characteristic for the 1,8-naphthalimide anion radical[3] and of bands at 359 nm, 485/520 nm and a broad band developing into NIR, which are characteristic of the coordinated bpy* radical anion.[30] This confirmed the data from cyclic voltammetry that bpy* and NAP ligands are reduced at very similar potential.

The spectral changes observed during the first and the second reduction processes of NDI and NAP-NDI complexes were very similar. The first reduction resulted in the depletion of the absorption bands of the 1,4,5,8-naphthalenedimiide and gave rise to the new bands that are characteristic of the

(30) Krejcik, M.; Vlcek, A. A. *J. Electroanal. Chem.* **1991**, *313*, 243.

1,4,5,8-naphthalenedimiide radical anion (Table 4). The second reduction led to the depletion of radical anion absorption bands and gave rise to the new bands at 600/608, 552/559, 423/423, and 400/400 nm for the NDI/NAP-NDI complexes, respectively, corresponding to the absorbencies of the dianion of 1,4,5,8-naphthalenedimiide.[6] Thus both LUMO and LUMO+1 in NDI and NAP-NDI complexes are 1,4,5,8-naphthalenedimiide-localized.

On the basis of the changes observed in the UV−vis absorption spectra in the course of third reduction, and of the CV data, the third reduction processes in Pt(bpy*)NDI is likely to be localized on the bpy*, and third/fourth reduction processes in Pt(bpy*)NAP-NDI are likely to be on the bpy*/1,8-naphthalimide. However, with the exception of the NAP complex, reductions based on bpy* for this series of compounds were not completely reversible in CH_2Cl_2 and were therefore investigated in DMF (Table 4b). The reduction of the parent compound, Pt(bpy*)Cl_2, was also investigated for comparison.

In DMF, the spectral changes observed during the first reduction process of the Pt(bpy*)(3,5-cat) and Pt(bpy*)PHT were very similar and are characteristic of the formation of the bpy*-radical anion. The second reduction of the PHT complex gives a general increase of optical density at wavelengths less than 465 nm, with a new peak at 442 nm, characteristic of the phthalimide radical anion. This implies that the LUMO is on the bpy*, and the LUMO+1 is on the phthalimide moiety in Pt(bpy*)PHT.

For the NDI complex in DMF, the first and second reduction processes gave the results essentially identical to the data obtained in CH_2Cl_2. The third reduction of the NDI complex was accompanied by the depletion of the absorption band at 295 nm and a formation of new spectral features characteristic of the coordinated bpy* radical anion (Figure 6).

EPR Spectroscopy. To provide insight into the electrochemical behavior of the Pt(bpy*)(cat-imide) compounds and on the nature of their frontier orbitals, EPR spectroscopic studies were carried out for the oxidized and reduced Pt(bpy*)(cat-imide) species at 298 and 77 K at 1 mM. Experimental and simulated EPR spectra are given in Figures 7−10, and data are summarized in Tables 5 (oxidation) and 6 (reduction). The system of coordinates used for EPR simulations is given in Figure 7.

EPR Spectroscopy of Oxidized Species. The mechanism of the oxidation proposed above on the basis of CV and UV−vis spectroelectrochemistry introduces formation of several intermediate species (Scheme 4), some of which would be EPR active ($S = ½$).

EPR studies were therefore carried out for two stages of the oxidation process: under 50% (corresponding to the removal of one electron per two Pt centers) and 100% (corresponding to the removal of one electron per Pt center). For each compound, 50% oxidation was accomplished either chemically, by the addition of 0.5 equivalents of [AcFc][BF_4], or electrochemically, and in each case, the form of the EPR spectrum was essentially independent of the preparative route. Complete oxidation was achieved by

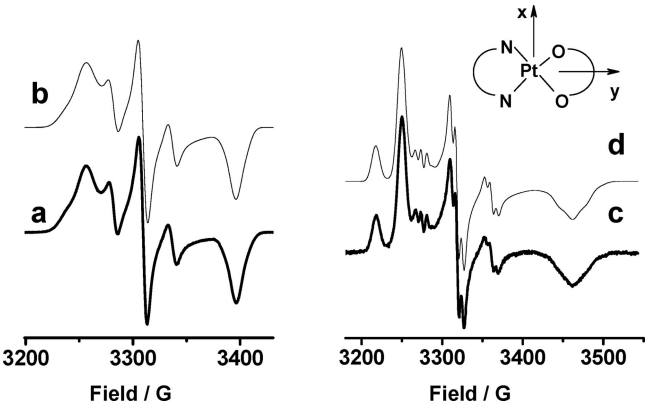

Figure 7. Experimental (a) and simulated (b) EPR spectra of 1 mM [Pt(bpy*)(3,5-cat)]$^+$ in CH_2Cl_2 containing [Bu_4N][PF_6] (0.4 M) at 77K. Experimental (c) and simulated (d) EPR spectra of 1 mM [Pt(bpy*)(3,5-cat)]$^-$ in DMF containing [Bu_4N][PF_6] (0.2 M) at 77K.

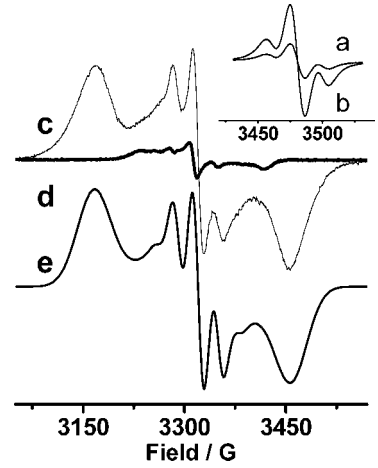

Figure 8. EPR spectra of electrochemically oxidized 1 mM Pt(bpy*)NDI complex in CH_2Cl_2 containing 0.4 M [Bu_4N][PF_6]: in fluid solution at 50% (a) and 100% (b) oxidation levels; in frozen solution at 77 K, at 50% (c) and 100% (d) oxidation levels; and (e) simulated spectrum for the monocationic dimeric species, $[MM]^{+\bullet}$, M = Pt(bpy*)NDI.

electrochemical methods. The results reported herein, both at 50% and 100% oxidation levels are taken from electrochemical experiments, with the exception of Pt(bpy*)(3,5-cat), which was generated chemically at the 100% oxidation level only.

Pt(bpy*)(cat-imide) and Oxidation Pathway in Fluid Solution at Ambient Temperature. For each Pt(bpy*)(cat-imide) compound at 298 K, the EPR spectra of fluid solutions at 50% and 100% oxidation levels were identical in all parameters except for relative intensity and virtually identical to the EPR spectrum of 100% oxidized Pt(bpy*)(3,5-cat) (Table 5). The spectral shape is consistent with the unpaired electron interacting with the Pt nuclei, taking into account standard isotopic distribution (Table 5). The value of the double integrated area increased nearly proportionally with the oxidation progressing from 50% to 100% (Figure 8), indicating that the oxidation process in bulk solution leads to only one type of EPR active species, namely, $[M]^{+\bullet}$.

In summary, the following interpretation of the oxidation processes of Pt(bpy*)(cat-imide) in fluid solution is proposed (Scheme 4). The CV experiment follows the processes in the diffusion layer and observes two consecutive oxidation

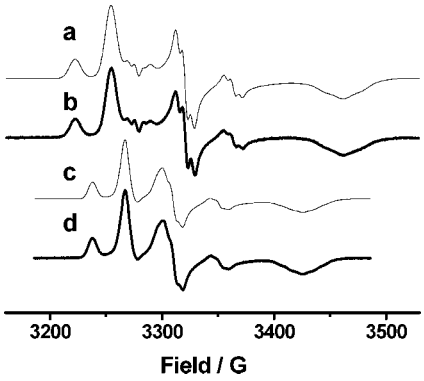

Figure 9. Simulated (a) and experimental (b) EPR spectra of 1 mM $[Pt(bpy^*)NDI]^{3-}$ in DMF containing $[Bu_4N][PF_6]$ (0.2 M) at 77 K. Simulated (c) and experimental (d) EPR spectra of $[Pt(bpy^*)Cl_2]^{-\bullet}$ in DMF containing $[Bu_4N][PF_6]$ (0.2 M) at 77 K.

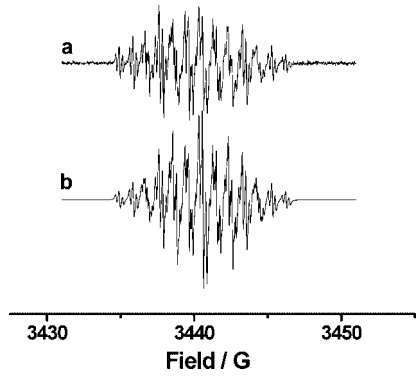

Figure 10. Experimental (a) and simulated (b) EPR spectra of 1 mM $[Pt(bpy^*)NDI]^{2-}$ in DMF containing $[Bu_4N][PF_6]$ (0.2 M) at 298 K.

events (Figure 4), amounting in total to a one-electron transfer. Those processes refer to the formation of [M] + $[M]^{+\bullet} \rightarrow [MM]^{+\bullet}$ dimer at first stage, which then undergoes a second electron transfer at potentials slightly more positive than that of the oxidation of [M], forming $[MM]^{2+}$. The EPR data, taken from electrogenerated samples, suggest that monomeric $[M]^{+\bullet}$ species dominate at ambient temperature in *bulk* fluid solution both at 50% and 100% oxidation (Scheme 4). This would imply that intermediate dimer species are unstable with respect to dissociation and the formation of monomer $[M]^{+\bullet}$. The UV−vis spectroelectrochemical data are consistent with this explanation: the band at 650 nm which first forms and then depletes in the course of oxidative electrolysis may be characteristic of these intermediate dimer species. Thus, $[MM]^{+\bullet}$ and $[MM]^{2+}$ are kinetic products, while thermodynamic product of oxidation in fluid solution appears to be monomeric $[M]^{+\bullet}$ in all cases. It is worth noting that the solution of neutral Pt(bpy*)(cat-imide) in CH_2Cl_2 at ambient temperature obeys the Beer–Lambert law in the concentration range up to 1 mM, indicating that aggregation only occurs in the course of oxidation. The structure of the proposed dimers can not be stated unambiguously on the basis of our data.[31]

The lack of dimerization observed in the course of the oxidation of Pt(bpy*)(3,5-cat) may be caused by the bulky ^{t}Bu-groups on the catecholate ligand, which prevent aggregation within the concentration range investigated.

Pt(bpy*)(3,5-cat) at 77 K. The model compound Pt(bpy*)(3,5-cat), upon 100% oxidation, yields a well-defined EPR spectrum (Figure 7a) at 77 K. This spectrum was assigned to the radical cation, $[Pt(bpy^*)(3,5\text{-cat})]^{+\bullet}$, with the unpaired electron localized predominantly on the catecholate ligand. Accordingly, the spectrum was simulated as a superposition of two rhombic EPR spectra, corresponding to the unpaired electron interacting with the Pt nuclei in standard isotopic distribution ($I = 0$, 66.2%; $I = ½$, from ^{195}Pt, 33.8%, Figure 7b), with the parameters very similar to that previously reported[17] for [Pt(4,7-diphenyl-1,10-phenanthroline)(3,5-cat)]$^{+\bullet}$ (Table 5). Hyperfine coupling was apparent at each principal axis, small in g_{zz}, out of the plane of the molecule, and largest in g_{xx}. The overall contribution from Pt $5d_{yz}$ and $6p_z$ orbitals, determined by the Reiger's methodology,[32,33] adopted as described previously,[17] constituted 7%. These data point unambiguously at the Pt d-orbitals participation in the SOMO of $[Pt(bpy^*)(3,5\text{-cat})]^{+\bullet}$.

It shall be noted that for experiments conducted at 77 K, the EPR spectrum of fully oxidized $[Pt(bpy^*)(3,5\text{-cat})]^{+\bullet}$ is strikingly different than the spectra of Pt(bpy*)(cat-imide) at 50% oxidation level but similar to the residual spectra observed for fully oxidized Pt(bpy*)(cat-imide).

For $[Pt(bpy^*)(3,5\text{-cat}))]^{+}$, there is a good agreement between g_{iso} (2.000) and g_{av} ($= {}^1/_3(g_{xx} + g_{yy} + g_{zz}) = 1.996$) and, A_{iso} (32×10^{-4} cm^{-1}) and A_{av} ($= {}^1/_3(A_{xx} + A_{yy} + A_{zz}) = 33 \times 10^{-4}$ cm^{-1}; this supports a lack of significant perturbation of the sample upon cooling. The good correlation between A_{iso} and A_{av} also indicate that the sign of the *A*-matrix components is the same throughout. The *g*-anisotropy ($g_{yy} - g_{zz} = 0.074$) and anisotropic hyperfine coupling constants (A_{xx}, A_{yy}, and A_{zz} = 32, 51, and 16×10^{-4} cm^{-1}, respectively) are small, especially when compared to oxidations of S-based analogues, [Pt(bpy*)(3,6-bis(trimethylsilyl)benzene-1,2-dithiolate)]$^{+\bullet}$ (Δg = 0.327; A_{xx}, A_{yy}, and A_{zz} = 200, 153, and 140×10^{-4} cm^{-1}, respectively).[34] These parameters reflect the larger contribution of S versus O atoms to the SOMO of the radical cation,

(31) Although the structure of the proposed dimers cannot be stated unambiguously on the basis of our data, three arrangements might be speculated upon: (i) imide−imide stacking, (ii) bpy*−bpy* stacking, and (iii) Pt−Pt interaction. The imide−imide and bpy*−bpy* stacking are unlikely because in that case the dimerization would occur also in the course of the reduction. The X-ray structure suggests a likelihood of Pt−Pt interaction in the dimers. The electronic communication within the dimer is evident from the CV data; therefore, the proposed dimer will be a delocalized one, with two equivalent Pt centers. In principle, delocalization of electron density between two Pt centers will be reflected in the reduction of the *A* values extracted from the EPR spectra of the dimeric vs monomeric oxidized species. However, the *A* values in the EPR spectra of oxidized species (Table 5) are virtually identical for Pt(bpy*)(cat-imide) and Pt(bpy*)(3,5-cat) complexes, suggesting only very small change of the electron density on the Pt centers upon dimerization. This is not unreasonable given the predominantly catechol-based nature of the oxidation, with only small (7%) contribution of Pt orbitals in the SOMO of oxidized species, which, if distributed equally between two Pt centers in $[MM]^{+\bullet}$ would not necessarily be apparent within the uncertainty of the simulation of the EPR spectra. It is therefore tentatively proposed that the dimers are formed by Pt−Pt interaction. The rate of dissociation of the dimer with the formation of the thermodynamic product, monomeric $M^{+\bullet}$, decreases with an increase of the size of the appended imide group.

(32) Rieger, P. H. *J. Magn. Reson.* **1997**, *124*, 140.
(33) McInnes, E. J. L.; Farley, R. D.; Rowlands, C. C.; Welch, A. J.; Rovatti, L.; Yellowlees, L. J. *J. Chem. Soc., Dalton Trans.* **1999**, 4203.

Table 5. EPR Spectroscopic Data for the Oxidized Forms of Pt^{II} Complexes upon 50 and 100% Oxidation [a]

complex	oxidation	g_{iso}	A_{iso}	g_{yy}	g_{xx}	g_{zz}	A_{yy}	A_{xx}	A_{zz}
3,5-cat	100%	2.000	32 (7)	2.038	2.005	1.954	32 (16)	51 (6.9)	16 (10)
NDI	50%	2.001	35 (10)	2.094	1.998	1.919	[b](48)	53 (12)	[b](38)
	100%[c]	2.001	35 (10)	2.051[d]	2.003	1.942	29[e](25)	57 (8)	16[e](18)
PHT	50%	2.000	34 (8)	2.081	1.998	1.925	[b](45)	54 (12)	[b](35)
	100%[c]	2.000	34 (8)	2.048	2.003	1.945	43[e](25)	53 (10)	16[e](15)
NAP	50%	2.001	35 (9)	2.090	1.998	1.921	[b](42)	53 (12)	[b](35)
	100%[c]	2.001	35 (9)	2.049[f]	2.003	1.941	29[e](25)	57 (10)	16[e](18)
NAP-NDI	50%			2.094	1.999	1.920	[b](46)	53 (12)	[b](39)
	100%[c]	2.001	35 (16)	2.050[g]	2.002	1.942	33[e] (25)	55 (10)	22 (15)

[a] One millimolar solutions in CH_2Cl_2 containing 0.4 M $[Bu_4N][PF_6]$ unless stated otherwise, $A/10^{-4}$ cm^{-1} (line width/G). [b] Not observed, simulated solely by line width. [c] Data from residual signal. [d] Additional signal at $g \approx 2.038$. [e] Estimated from the line shape. [f] Additional signal at approximately g ≈ 2.036. [g] Spectrum contained a mixture of peaks assigned as both fully and half oxidized products.

Table 6. EPR Spectroscopic Data for the Reduced Forms of Pt^{II} Complexes

complex	g_{iso}	A_{iso}	g_{yy}	g_{xx}	g_{zz}	A_{yy}	A_{xx}	A_{zz}
$(3,5\text{-cat})^-$	1.987	59 (18)	2.040	1.998	1.915	−61 (10)	−80 (4.5)[b]	−32 (15)[c]
NDI^-	2.005	[d]						
NDI^{2-}	2.005	[e]						
NDI^{3-}	1.989		2.038	1.998	1.916	−61 (10)	−80 (4.5)[f]	−32 (15)[c]
PHT^-	1.987	59(16)	2.037[g]	1.998	1.919	−61 (10)	−81 (4.5)[f]	−32 (15)[c]
PHT^{2-}	1.986	52(26)						
	2.004	2.3(0.8)[h]						
$[Pt(bpy^*)Cl_2]^{-a}$	1.992	49 (15)	2.031	2.004	1.937	−55 (7.5)	−77 (5.2)[f]	−15 (10)[h]

[a] One millimolar solution in DMF containing 0.2 M $[Bu_4N][PF_6]$, $A/10^{-4}$ cm^{-1} (line width/G). [b] Additional coupling $a_{2H} = 6.1 \times 10^{-4}$ cm^{-1}. [c] Additional coupling $a_{2H} = 13.4 \times 10^{-4}$ cm^{-1}. [d] $a_{2H} = 1.882$, $a_{2H} = 1.648$, $a_{2N} = 0.885$, $a_{2H} = 0.213$, Lorentzian line shape, 0.13 G line width. [e] $a_{2H} = 1.881$, $a_{2H} = 1.647$, $a_{2N} = 0.885$, $a_{2H} = 0.213$, Lorentzian line shape, 0.10 G line width. [f] Additional coupling $a_{2H} = 5.6 \times 10^{-4}$ cm^{-1}. [g] Additional line at approximately $g = 2.004$ in 77 K spectrum, possibly the result of a phthalimide-based radical. [h] Additional coupling $a_{2N} = 9.0 \times 10^{-4}$ cm^{-1}.

Scheme 4. Proposed Processes Accompanying Oxidation of M = Pt(bpy*)(cat-imide) in CH_2Cl_2

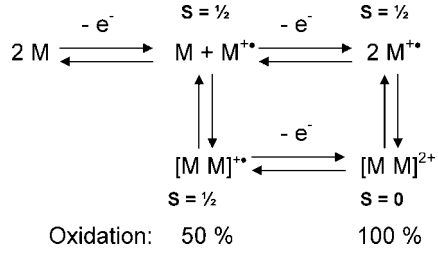

consistent with the DFT calculations for various Pt(bpy)(dithiolate) complexes, and indicate a HOMO that is predominantly sulfur 3p-character.[34,35]

Pt(bpy*)(cat-imide) at 77 K. In a sharp contrast to the fluid solution data, the form of the EPR spectra obtained from the solutions cooled to 77 K were dependent on the oxidation level. For all Pt(bpy*)(cat-imides), the EPR spectra obtained under 50% oxidation were dramatically depleted in intensity and changed upon complete oxidation. Figure 8a and b shows an example of such a change for Pt(bpy*)NDI; the double-integrated EPR spectrum for the 100% oxidized complex gave a value of less than 10% of the corresponding value for the 50% oxidized species. The low-intensity EPR spectra of 100% oxidized $[Pt(bpy^*)(cat\text{-}imide)]^{+\bullet}$ are similar in the spectral shape to that of $[Pt(bpy^*)(3,5\text{-}cat)]^{+\bullet}$. Hence, it is proposed that the EPR spectrum observed upon complete one-electron oxidation is a residual spectrum of a monomeric radical cation.

EPR spectra of 50% oxidized Pt(bpy*)(cat-imide) appear to have rhombic form (Figure 8c). Features assigned as g_{yy} and g_{zz} are broad, and hyperfine coupling, presumably caused by Pt, is apparent only in g_{xx}, where it takes values very similar to that for $[Pt(bpy^*)(3,5\text{-}cat)]^{+\bullet}$ ($\sim 51 \times 10^{-4}$ cm^{-1}). Again, the g-anisotropy and anisotropic hyperfine coupling constants are small, especially when compared to oxidations of S-based analogues,[34] such that no hyperfine coupling was resolved in g_{yy} or g_{zz}, and these features were simulated by the line width.

There are several possibilities for the assignment of the EPR spectra of 50%-oxidized species at 77 K, including solely a monomer, solely a dimer formed as a result of aggregation of monomeric $[M]^{+\bullet}$ with [M] upon cooling, or a multicomponent system including both a monomer and a dimer.[36] We favor the latter because it is consistent with the data of CV and UV−vis (spectro)electrochemistry, as described in detail below.

The assignment of the spectrum of 50%-oxidized species to a monomeric $[Pt(bpy^*)(cat\text{-}imide)]^{+\bullet}$ solely is unlikely, given the drastic difference between the EPR spectra under 50% and 100% oxidation and the similarity of the latter with that of $[Pt(bpy^*)(3,5\text{-}cat)]^{+\bullet}$.

Simulation of the experimental spectra at 50% oxidation level solely as the monocationic dimer species, $[Pt(bpy^*)(cat\text{-}imide)]_2^{+\bullet}$, using a statistical distribution of spin active Pt isotopes ($^{193}Pt^{193}Pt$, 43.8%; $^{193}Pt^{195}Pt$, 44.8%; $^{195}Pt^{195}Pt$, 11.4%) and Gaussian line shape reproduced the major spectral features only (Figure 8e). There are small features in the experimental spectra of the 50% oxidized species

(34) Pap, J. P.; Benedito, F. L.; Bothe, E.; Bill, E.; George, S. D.; Weyhermüller, T.; Wieghardt, K. *Inorg. Chem.* **2007**, *46*, 4187.

(35) Zuleta, J. A.; Bevilacqua, J. M.; Prosperio, D. M.; Harvey, P. D.; Eisenberg, R *Inorg. Chem.* **1992**, *31*, 2396.

(36) We have also considered a possibility that the form of the 50% oxidized spectra represent a triplet ($S = 1$) species with significant rhombic distortion ($E/D \approx 1/3$). However, simulation of the experimental data as $S = 1$ species failed to give an adequate reproduction of the observed spectra, and those parameters gave a simulated half-field signal that was not found experimentally, even at the high spectrometer gain that was indicated by the results of the simulation.

(Figure 8c) that were not reproduced by the simulation solely for $[Pt(bpy^*)(cat\text{-}imide)]_2^{+\bullet}$ dimers but that correspond well to the position of peaks noted in the 100% oxidized spectra, which were attributed to the monomer $[Pt(bpy^*)(cat\text{-}imide)]^{+\bullet}$ (Figure 8d). In effect, the experimental EPR spectra at 50% oxidation are reproducible by a combination of the EPR spectra simulated separately for dimer $[MM]^{+\bullet}$ and monomer $[M]^{+\bullet}$. This leads to the assumption of an (equilibrium) mixture between $[M]^{+\bullet}$ and $[MM]^{+\bullet}$ formed in the 50% oxidized fluid solution upon cooling to 77 K.

Thus we conclude that EPR spectra for Pt(bpy*)(cat-imide) complexes at 77 K are consistent with a combination of $S = ½$ species, $[M]^{+\bullet}$ and $[MM]_2^{+\bullet}$ for 50% oxidation and with a combination of $S = ½$ species, $[M]^{+\bullet}$ and EPR-silent dimers $[MM]_2^{2+}$ ($S = 0$), for 100% oxidation. The weak signal observed in frozen solution for 100% oxidation represents the residual $[M]^{+\bullet}$ component of a $[M]^{+\bullet} - [MM]_2^{2+}$ equilibrium in fluid solution, which has not been shifted completely toward $[MM]_2^{2+}$ upon cooling.

Therefore, in contrast to the studies of oxidation processes at ambient temperature, where the dimers appear to be formed either in the diffusion layer (CV) or as transient species in UV−vis spectroelectrochemistry, the formation of dimer $[MM]_2^{+\bullet}$ and $[MM]_2^{2+}$ species at 77 K occurs as a result of the aggregation of $[M]^{+\bullet}$ radicals upon cooling of the bulk fluid solutions.

The precedent for such behavior has been reported recently for Pt(bpy*)(1,2-bis(4-*tert*-butylphenyl)ethylene-1,2-dithiolate),[34] while this work was in progress.

EPR Spectroscopy of Reduced Species. The electrochemically generated radical anions of 3,5-cat, PHT, and NDI complexes were investigated by EPR spectroscopy in DMF solution. The one-electron reduction of the parent compound, $Pt(bpy^*)Cl_2$ was also studied. The parameters used in simulations of the experimental spectra are summarized in Table 6.

The EPR spectra of one-electron reduced 3,5-cat and PHT complexes and of three-electron reduced NDI complex are very similar to each other in both fluid (298 K) and frozen (77 K) solutions (Figure 7c and d and Figure 9).

In each case the room temperature spectrum was consistent with the coupling of an unpaired electron with a Pt nucleus; no superhyperfine coupling was resolved.

The 77 K spectra are rhombic and consistent with the generation of a radical anion based primarily on bpy*, with some contribution from the metal-based orbitals. The total Pt contribution from $5d_{yz}$ and 6_{pz} orbitals was estimated as ~10%, with the 6_{pz} contributing more significantly (6%) than the $5d_{yz}$ to the SOMO. This low metal contribution confirms the predominantly ligand (bpy*) character to the orbital, which was further evidenced by resolution of superhyperfine in the g_{xx} and g_{zz} components of the spectra. This superhyperfine coupling was reproduced by inclusion of two equivalent hydrogen atoms into the simulation parameters and attributed to the C5,5′-positions of bpy* which are expected to give rise to the largest splitting.

The observation of superhyperfine coupling yields spectra of the form remarkably similar to that reported for Pt(2,2′-bipyrimidine)Cl_2,[37] where the coupling was assigned to the hydrogen atoms in the 5,5′ positions of 2,2′-bipyrimidine. Coupling of the unpaired electron to hydrogen atoms of bpy as measured for $[Pt(4,4'\text{-}CO_2Me\text{-}bpy)Cl_2]^-$ by ^1H ENDOR spectroscopy also demonstrated that the C5,5′ positions of bpy carried 30% of the unpaired electron density.[33]

For $[Pt(bpy^*)Cl_2]^-$, the EPR spectrum at 77 K also shows some superhyperfine coupling, although the slight increase in line width for g_{xx} tended to reduce its resolution. Interestingly, in this case, the superhyperfine coupling in g_{zz} was best reproduced by inclusion of two equivalent nitrogen atoms into the parameters of the simulation, a result consistent with the simulation parameters for the frozen EPR spectrum of $Pt(bpy)Cl_2$. The calculated Pt contribution to the SOMO in $[Pt(bpy^*)Cl_2]^{-\bullet}$ was 13%, consistent with that for other $[Pt(4,4'\text{-}X_2\text{-}bpy)Cl_2]^-$ (X = OEt, Me, Ph, H, Cl, CO_2Me) species.[38] As could be anticipated, the electron-donating group (^{t}Bu, Hammett parameter $\sigma_p = -0.20$) increased the contribution of the Pt $6p_z$ orbital to the SOMO versus $5d_{yz}$ (8.3% $6p_z$; 4.7% $5d_{yz}$), thus lowering the g anisotropy.

In general, the reduced Pt(bpy*)(catecholate) species show smaller Pt $6p_z$ contribution in the SOMO, higher g-anisotropy, slightly lower g_{iso} values but larger ^{195}Pt hyperfine coupling constants than the parent dichloride compound. These facts are consistent with the catecholato group being less electron withdrawing than chloride, as was evident from the potentials of the bpy*-based reduction in Pt(bpy*)(cat-imide) (−1790 to −1820 mV, Table 3) versus that of $Pt(bpy^*)Cl_2$ (−1700 mV).

EPR spectroscopy was used to assign the two partially overlapping reduction processes detected for Pt(bpy*)PHT by cyclic voltammetry. The first one-electron reduction leads to an EPR spectrum (Figure 13S) that shows features typical for an unpaired electron localized on the bpy*; hence first reduction is assigned primarily as bpy*-based. A small additional signal, at $g \approx 2.005$, observed in the spectra at both 298 and 77 K, was assigned to the presence of a radical anion based on the phthalimide group appended to the catecholate. The presence of this signal probably represents a small contribution from $[Pt(bpy^{*\bullet})PHT^\bullet]^{2-}$ to the thermodynamic equilibrium between Pt(bpy*)PHT, $[Pt(bpy^{*\bullet})PHT]^-$, and $[Pt(bpy^{*\bullet})PHT^\bullet]^{2-}$for a one-electron reduced solution of Pt(bpy*)PHT, given the close proximity of the two reduction processes.

The two-electron reduction of Pt(bpy*)PHT generates a biradical, $[Pt(bpy^{*\bullet})PHT^\bullet]^{2-}$ (Figure 14S). Fluid solution EPR spectrum shows clearly the superposition of a five line spectrum, simulated as coupling to four equivalent hydrogen atoms (likely those of the phthalimide moiety), and the spectrum of an unpaired electron coupled to a Pt center, likely to be bpy* based.

For Pt(bpy*)NDI, both the first and second reduction processes are based on the 1,4,5,8-naphthalenedimiide group appended to the catechol ligand (Figure 10). One-electron

(37) Kaim, W.; Dogan, A.; Wanner, M.; Klein, A.; Tiritiris, I.; Schleid, T.; Stufkens, D. J.; Snoeck, T. L.; McInnes, E. J. L.; Fiedler, J.; Záliš, S. *Inorg. Chem.* **2002**, *41*, 4139.

reduction yielded the spectrum corresponding to the 1,4,5,8-naphthalenedimiide radical anion, the fluid solution EPR spectrum of which was simulated by an unpaired electron interacting with three pairs of hydrogen atoms and two equivalent nitrogen atoms.[39]

Concluding Remarks

It has been shown that catecholate ligands can be easily modified with an electron-accepting imide group without changing their coordination capability. This property was illustrated by the synthesis of the stable Pt^{II} diimine catecholate complexes, which combine optical (absorption) and electrochemical properties of both the cathecol and the imide units.

A combination of UV−vis absorption spectroscopy, cyclic voltammetry, UV−vis spectroelectrochemistry, and EPR spectroscopy has allowed for the assignment of the nature of frontier orbitals in Pt(bpy*)(cat-imide) complexes. The HOMO in Pt(bpy*)(cat-imide) is centered on the catechol ligand, while the LUMO is localized either on bpy*, or on the imide group, depending on the nature of the imide group involved. The LUMO is centered on the bpy* ligand for 3,5-cat, PHT, and NAP complexes and on the 1,4,5,8-naphthalenedimiide group in the NDI and NAP-NDI complexes.

Despite the variations in the nature of the LUMO, the lowest-detectable electronic transition in all Pt(bpy*)(cat-imide) complexes has predominantly catechol-to-diimine charge-transfer nature (LLCT). This transition involves a bpy*-based unoccupied molecular orbital in all cases, that is, LUMO for the 3,5-cat, PHT, and NAP complexes, LUMO+2 for the NDI and LUMO+2 (or LUMO+3) for the NAP-NDI complexes. This conclusion is consistent with a lack of the electronic communication between the catechol and the imide groups in the Pt(bpy*)(cat-imide) complexes, which could be anticipated on the basis of the near orthogonal orientation of these groups in the solid state.

The LLCT transition in all Pt(bpy*)(cat-imide) complexes appears at 530 nm in CH_2Cl_2, with an extinction coefficient of $\sim 6 \times 10^3$ L mol^{-1} cm^{-1}, and is strongly negatively solvatochromic: these charactertistics are most similar to those reported previously for other Pt^{II} diimine catecholate complexes and for the model compound Pt(bpy*)(3,5-cat). The energy of the lowest charge-transfer transition is remarkably insensitive to the imide group present, indicating once again the lack of electronic communication between the imide and the catechol units. This feature opens up future possibilities for optimizing various molecular properties though peripheral modification of the imide without altering the absorption properties of the [diimine-Pt-catechol] core.

The Pt(bpy*)(cat-imide) complexes show up to four reversible redox processes within the accessible potential range (from −2 to +1 V), which, coupled with intense absorptions of their neutral, reduced, and oxidized forms, and a highly solvatochromic LLCT transition, renders these compounds promising electrochromic materials.

It is suggested that dimerization determines the ECEC mechanism of the oxidation in the diffusion layer in the course of cyclic voltammetry experiments, which might explain the concentration- and solvent-dependent oxidation behavior.

The Pt orbitals contribution into the SOMO of the reduced species was estimated as ∼10–13% from the analysis of the EPR spectroscopic data. The Pt orbitals contribution in the SOMO of the radical cation is somewhat smaller, 7% for $[Pt(bpy^*)(3,5\text{-cat})]^{+\bullet}$. The Pt contribution in the frontier orbitals accounts for the high extinction coefficient of the corresponding lowest-allowed catecholate-to-bpy* electronic transition. The radical cations of Pt(bpy*)(cat-imide) are characterized by lower degree of *g*-anisotropy than that reported previously for radical-cations of Pt(diimine)(thiolate) complexes, indicating a smaller contribution of O versus S atoms to the SOMO.

The modular variation of the diimine, catechol, imide, and central metal will make accessible a wide range of redox states and of broadly tuneable absorption properties in the metal diimine catechol-imide and metal catechol-imide complexes in general.

The synthetic approach to imide-modified catechols described herein could potentially be extended to a preparation of poly catechol ligands with future application in supramolecular chemistry and to an incorporation of any suitable imide group in molecular assemblies.

Experimental Section

In-house facilities were used for CHN and EI MS analysis. The following instruments were used: absorption spectra, a Cary 50 Bio UV–visible spectrophotometer; luminescence spectra, a Perkin-Elmer LS 50B spectrofluorimeter; ^{1}H NMR spectra (presented as δ in ppm and J in Hz), a Bruker 250 MHz spectrometer. EPR spectra were recorded on a Bruker EMX spectrometer, and spectral simulations were accomplished using WINEPR SimFonia, version 1.25, software. The concentration of the samples for EPR studies obtained by bulk electrolysis was 1 mM.

Standard cyclic and square-wave voltammetric and coulometric studies were carried out using an Autolab PGSTAT20 potentiostat. The voltammetry was carried out under an atmosphere of argon using a three-electrode arrangement in a single compartment cell. A glassy carbon working electrode, a Pt wire secondary electrode, and a saturated calomel reference electrode, chemically isolated from the test solution via a bridge tube containing electrolyte solution and fitted with a porous vycor frit, were used in the cell.

(38) McInnes, E. J. L.; Farley, R. D.; Macgregor, S. A.; Taylor, K. J.; Yellowlees, L. J.; Rowlands, C. C. *J. Chem. Soc., Faraday Trans.* **1998**, *94*, 2985.

(39) The second reduction results in a spectrum essentially identical in shape but depleted relative to that obtained for the one-electron reduced species (∼20% of the one-electron reduced species by double integration of spectra). The spectra of doubly reduced Pt(bpy*)NDI can be simulated with the same hyperfine parameters as $[Pt(bpy^*)NDI]^{-\bullet}$ albeit with a slightly reduced line width (a possible consequence of effectively using a more magnetically dilute sample, thus reducing dipolar broadening effects), consequently the spectrum of the two electron reduced species appears better resolved and is used as a representative spectrum. The signal observed for the two-electron reduced species is considered to represent a residual component arising from the presence of monoanion radical, with the majority product, the dianion $[Pt(bpy^*)NDI]^{2-}$, as an EPR silent, $S = 0$, species resulting from the spin pairing of electrons in the 1,4,5,8-naphthalenediimide group orbital manifold. This residual signal is not apparent in either fluid or frozen solution spectra of the three electron reduced species, suggested some reoxidation had occurred during sample preparation at the two-electron reduced level.

The solutions were 10^{-3} M in the test compound unless stated otherwise; $[NBu_4][BF_4]$ (0.4 M for CH_2Cl_2 and 0.2 M for DMF) was used as supporting electrolyte. The redox potentials are quoted versus the ferrocenium-ferrocene couple, decamethylferrocene was used in each experiment as an internal standard. $E_{1/2}$ of decamethylferrocene versus Fc^+/Fc was -0.535 V, under these conditions. Coulometric studies, at a controlled potential, were carried out using a two-compartment cell. The Pt/Rh gauze basket working electrode was separated from the wound Pt/Rh gauze secondary electrode by a glass frit. A saturated calomel reference electrode was bridged to the test solution through a vycor frit orientated at the center of the working electrode. The working electrode compartment was fitted with a magnetic stirrer bar, and the test solution was stirred rapidly during electrolysis. The UV−vis spectroelectrochemical experiments were carried out on ~0.5 mM solutions in optically transparent electrochemical (OTE) cell (modified quartz cuvette, with 0.5 mm optical path length). The cell comprised a three-electrode configuration, consisting of a Pt/Rh gauze working electrode, a Pt wire secondary electrode (in a fritted PTFE sleeve) and a saturated calomel electrode, chemically isolated from the test solution via a bridge tube containing electrolyte solution and terminated in a porous frit. The potential at the working electrode was controlled by a Sycopel Scientific Ltd. DD10 M potentiostat. The (spectro)electrochemical UV−vis data were recorded on a Perkin-Elmer Lambda 16 spectrophotometer. The cavity was purged with dinitrogen and temperature control at the sample was achieved by flowing cooled dinitrogen across the surface of the cell. Acetyl ferrocene tetrafluoroborate, $[AcFc][BF_4]$, was prepared as described previously.[40]

Nanosecond flash photolysis studies were performed on a home-built setup with a Nd:YAG laser (9 ns pulse width), a steady-state Xe lamp (Hamamatsu L 2273), a Hamamatsu PMT R928, and a Tektronix 3032B oscilloscope.

Synthesis. All reactions were carried out in the dark under atmosphere of nitrogen using general grade solvents that were degassed by bubbling nitrogen for 10 min. Purification, crystal growth, and handling of all compounds were carried out under air with a minimum exposure to light. All products were air- and moisture-stable solids which were stored in the dark when not in use.

Silica gel for flash chromatography (DAVISIL) was supplied by Fluorochem Ltd. (catalogue number LC301, 40–63 μm).

Synthesis of *N*-Octyl-1,4,5,8-naphthalenetetracarboxylic Monoanhydride. The synthesis is based on the reported procedure,[41] which was significantly modified. *n*-Octylamine (at least 2 mL, 1.56 g, 12 mmol, excess) was added to a suspension of 1,4,5,8-naphthalenetetracarboxylic dianhydride (1g, 3.73 mmol) in a mixture of water (10 mL) and *n*-propanol (10 mL) at RT under N_2. The suspension dissolved in 10 min, and the resulting solution was heated at 50 °C (important) for 24 h to give a white precipitate (the mixture was sonicated a few times in the first 2 h of reaction to ensure complete dissolution of dianhydride). The reaction mixture was cooled down to RT, acidified to pH 1 with HCl to give more precipitate, and was then further stirred for 1 h. The solid was filtered and stirred in acetic acid (100 mL or more) at reflux for 1 h or longer, producing first a suspension and then a clear yellow solution. It was cooled to RT (a precipitate might form on cooling), diluted with CH_2Cl_2 (200 mL), and extracted with water (200 mL) to give clear organic and aqueous layers (the formation of an inseparable emulsion at this stage can be avoided by addition of more acetic acid). The organic layer was separated and filtered (if required) to remove insoluble solid, an unreacted dianhydride. The organic layer was dried if required ($MgSO_4$) and then reduced in volume. The addition of ethanol (50 mL) and evaporation of CH_2Cl_2 gave a suspension of the product in ethanol that was filtered and washed with ethanol, hexane, and small amount of ether.

The product was obtained as a 1:12 molar mixture of the bis- and monoimide and was used without further purification (the bisimide is an inert impurity which is easily removed in the next reaction step). Crude yield = 0.99 g, containing 0.90 g (2.38 mmol, 64%) of monoimide. The product was obtained as a white or pale pink solid, $C_{22}H_{21}NO_5$ (M.W. 379.41), which was soluble in CH_2Cl_2 and acetone and insoluble in ethanol and hexane. Characteristic ^{1}H NMR ($CDCl_3$) signals were observed in aromatic region for the monoimide at 8.81 ppm (s) and for the bisimide at 8.75 ppm (s).

The reaction provided monoanhydride in a similar yield and purity when higher excess of *n*-octylamine were used (up to 4 mL of amine for 1 g of dianhydride). The advantage of using a higher excess of amine (up to 4 mL instead of 2 mL for 1 g of dianhydride) is faster reaction rate, easier handling and workup of the reaction mixture and better reproducibility of the product yield. It should be noted that the amount of bisimide impurity increases if the reaction is carried out at temperatures higher than 50 °C.

Synthesis of Methyl-Ether-Protected Catechols MeO-catimide. 4-Aminoveratrole and the corresponding aromatic carboxylic acid anhydride in 1:1 molar ratio were refluxed at 140 °C in dry and degassed DMF (5–8 mL) under nitrogen for 24 h. The reaction mixture sometimes solidified during the first 3 h of reaction. In that case more DMF was added. Cooling to RT and addition of ethanol (10 mL) yielded precipitate of the product that was filtered and washed with ethanol, acetone (10 mL), and ether. The products thus obtained were analytically pure and did not require further purification unless stated otherwise. The products were obtained as solids that were soluble in CH_2Cl_2 and $CHCl_3$ and were insoluble in ether, alcohols, and alkanes.

MeO-PHT. 4-Aminoveratrole (1.034 g, 6.8 mmol) and phthalic anhydride (1 g, 6.8 mmol) gave 1.56 g (5.5 mmol, 81%) of white product. Calcd for $C_{16}H_{13}NO_4$ (MW 283.28): C, 67.84; H, 4.63; N, 4.94. Found: C, 67.77; H, 4.33; N, 4.72. EI MS *m*/*z*: 283 (100%, M^+). ^{1}H NMR ($CDCl_3$): δ 3.89 (s, 3H), 3.92 (s, 3H), 6.92 (t, br, 1H), 6.97–6.99 (m, 2H), 7.74–7.83 (m, 2H), 7.90–7.99 (m, 2H).

MeO-NAP. 4-Aminoveratrole (0.77 g, 5.0 mmol) and 1,8-naphthalic anhydride (1 g, 5.0 mmol) gave 1.33 g (4.0 mmol, 80%) of white product. Calcd for $C_{20}H_{15}NO_4$ (MW 333.34): C, 72.06; H, 4.54; N, 4.20. Found: C, 71.67; H, 4.25; N, 4.22. EI MS *m*/*z*: 333 (100%, M^+). ^{1}H NMR ($CDCl_3$): δ 3.88 (s, 3H), 3.94 (s, 3H), 6.81 (d, *J* 2.2, 1H), 6.89 (dd, *J* 8.6, 2.4, 1H), 7.02 (d, *J* 8.5, 1H), 7.75–7.85 (m, *J* 8.3, 7.3, 2H), 8.27 (dd, *J* 8.6, 1.2, 2H), 8.65 (dd, *J* 7.3, 1.2, 2H).

MeO-NAP-NO$_2$. 4-Aminoveratrole (0.63 g, 4.1 mmol) and 3-nitro-1,8-naphthalic anhydride (1 g, 4.1 mmol) gave 1.28 g (3.38 mmol, 83%) of orange product. Calcd for $C_{20}H_{14}N_2O_6$ (MW 378.34): C, 63.49; H, 3.73; N, 7.40. Found: C, 63.20; H, 3.49; N, 7.26. EI MS *m*/*z*: 378 (100%, M^+). ^{1}H NMR ($CDCl_3$): δ 3.88 (s, 3H), 3.95 (s, 3H), 6.80 (d, *J* 2.2, 1H), 6.89 (dd, *J* 8.6, 2.4, 1H), 7.04 (d, *J* 8.6, 1H), 7.98 (m, *J* 8.2, 7.3, 1H), 8.48 (dd, *J* 8.3, 1.2, 1H), 8.83 (dd, *J* 7.3, 1.2, 1H), 9.19 (d, *J* 2.4, 1H), 9.35 (d, *J* 2.4, 1H).

MeO-NDI. 4-Aminoveratrole (0.5 g, 3.26 mmol) and *N*-octyl-1,4,5,8-naphthalenetetracarboxylic monoanhydride (1.24 g, 3.26 mmol) gave 1.15 g (2.23 mmol, 69%) of orange product after purification by column chromatography (SiO_2, 0.1–0.3% CH_3OH in CH_2Cl_2). Calcd for $C_{30}H_{30}N_2O_6$ (MW 514.57): C, 70.02; H, 5.88;

(40) Connelly, N. G.; Geiger, W. E. *Chem. Rev.* **1996**, *96*, 877.
(41) Nagao, Y.; Misono, T. *Bull. Chem. Soc. Jpn.* **1981**, *54*, 1191.

N, 5.44. Found: C, 69.95; H, 5.68; N, 5.32. EI MS *m/z*: 514 (100%, M^+). ^{1}H NMR ($CDCl_3$): δ 0.82–0.92 (m, br, 3H), 1.2–1.5 (m, br, 10H), 1.67–1.83 (m, br, 2H), 3.88 (s, 3H), 3.96 (s, 3H), 4.15–4.25 (t, br, 2H), 6.81 (d, *J* 2.5, 1H), 6.89 (dd, *J* 8.6, 2.5, 1H), 7.04 (d, *J* 8.6, 1H), 8.80 (s, 4H).

Synthesis of MeO-BTC. 4-Aminoveratrole (0.72 g, 4.7 mmol, small excess) and 1,2,4,5-benzenetetracarboxylic acid dianhydride (0.5 g, 2.29 mmol) were refluxed at 140 °C in dry and degassed DMF (8 mL) under nitrogen for 24 h. Cooling to RT gave precipitate of the product that was filtered and washed with ethanol and ether to give a bright yellow solid. Yield: 0.916 g (1.88 mmol, 82%). Calcd for $C_{26}H_{20}N_2O_8$ (MW 488.45): C, 63.93; H, 4.13; N, 5.74. Found: C, 63.75; H, 3.78; N, 5.64. EI MS *m/z*: 488 (100%, M^+). ^{1}H NMR ($CDCl_3$): δ 3.91 (s, 6H), 3.94 (s, 6H), 6.95 (d, br, 2H), 7.00–7.03 (m, 4H), 8.46 (s, 2H).

Synthesis of MeO-NAP-NH$_2$. This reaction was not sensitive to the presence of moisture in the reagents or the solvents used. A mixture of MeO-NAP-NO_2 (345 mg, 0.91 mmol), ammonium formate (1 g, 16 mmol, excess), and Pd/C (20 mg, catalyst) in degassed methanol (15 mL) under nitrogen at RT was sonicated for 30 min and refluxed for 6 h to give a dark yellow suspension. The reaction mixture was evaporated to dryness and dissolved in 200 mL of CH_2Cl_2. The organic phase was washed with water (2 × 100 mL), dried ($MgSO_4$), filtered though Celite to remove Pd/C, and evaporated to dryness to give pure product as a dark yellow solid. Yield: 287 mg (0.82 mmol, 91%). Calcd for $C_{20}H_{16}N_2O_4$ (MW 348.35). The compound is soluble in CH_2Cl_2, DMF, and DMSO; its solutions are luminescent. EI MS *m/z*: 348 (100%, M^+). ^{1}H NMR (DMSO-d_6): δ 3.71 (s, 3H), 3.82 (s, 3H), 5.97–6.04 (m, br, 2H), 6.85 (dd, *J* 8.6, 2.4, 1H), 6.99 (d, *J* 2.2, 1H), 7.04 (d, *J* 8.6, 1H), 7.30 (d, *J* 2.5, 1H), 7.63 (t, *J* 7.6, 1H), 7.96 (d, *J* 2.2, 1H), 8.03–8.10 (m, 2H).

Synthesis of MeO-NAP-NDI. MeO-NAP-NH_2 (287 mg, 0.82 mmol) and *N*-octyl-1,4,5,8-naphthalenetetracarboxylic monoanhydride (312 mg, 0.82 mmol) were refluxed at 140 °C in dry and degassed DMF (5 mL) under nitrogen for 24 h. Cooling to RT and the addition of ethanol (5 mL) gave precipitate of the product that was filtered, washed with ethanol and ether, and purified by column chromatography (20 g of SiO_2, 0.2–0.6% CH_3OH in CH_2Cl_2). A light-brown solid resulted. Yield: 391 mg (0.55 mmol, 67%). Calcd for $C_{42}H_{35}N_3O_8$ (MW 709.74): C, 71.07; H, 4.97; N, 5.92. Found: C, 70.43; H, 4.83; N, 5.82. EI MS *m/z*: 709 (100%, M^+). ^{1}H NMR ($CDCl_3$): δ 0.83–0.92 (m, 3H), 1.22–1.50 (m, 10H), 1.7–1.85 (m, 2H), 3.88 (s, 3H), 3.94 (s, 3H), 4.17–4.27 (m, 2H), 6.82 (d, *J* 2.4, 1H), 6.90 (dd, *J* 8.6, 2.4, 1H), 7.03 (d, *J* 8.9, 1H), 7.88 (m, *J* 8.3, 7.7, 1H), 8.28 (d, *J* 2.1, 1H), 8.32 (dd, *J* 8.6, 0.9, 1H), 8.56 (d, *J* 1.8, 1H), 8.74 (dd, *J* 7.3, 0.9, 1H), 8.81–8.89 (m, 4H).

Synthesis of Imide-Substituted Catechols by Deprotection of MeO-cat-imide with BBr$_3$. The appropriate bismethyl ether of catechol was suspended in dry and degassed CH_2Cl_2 (5 mL) under nitrogen and cooled in a dry ice−acetone bath. To this solution or suspension was added a 1.0 M solution of BBr_3 in CH_2Cl_2 (excess). The reaction mixture was warmed up and stirred at RT with occasional sonication for 24 h under nitrogen. The resulting suspension was cooled in a dry ice−acetone bath and was cautiously quenched with methanol (10–20 mL) (**CAUTION!** *Exothermic reaction*). The reaction mixture was warmed up to RT, followed by the addition of water (10 mL) and evaporation of CH_2Cl_2. More water (50 mL) was added to the resulting suspension, and it was stirred for 1 h. The product was filtered and washed with water and either ether or a 9:1 mixture of ether and ethanol. The compounds did not require further purification. The catechols were obtained as solids that were soluble in DMSO and DMF and were insoluble in hexane, ether, or water.

PHT. MeO-PHT (520 mg, 1.84 mmol) and BBr_3 (15 mL of 1 M solution in CH_2Cl_2) gave 297 mg (1.02 mmol, 55%) of yellow product. The compound has significant solubility in methanol, acetone, and ether. Calcd for $C_{14}H_9NO_4\cdot(H_2O)_2$ (MW 291.26): C, 57.73; H, 4.50; N, 4.81. Found: C, 58.21; H, 4.46; N, 4.67. EI MS *m/z*: 255 (100%, M^+). ^{1}H NMR (DMSO-d_6): δ 6.65 (dd, *J* 8.6, 2.5, 1H), 6.78 (d, *J* 2.2, 1H), 6.81 (d, *J* 8.6, 1H), 7.84–7.95 (m, 4H), 9.20–9.26 (m, 2H).

NAP. MeO-NAP (500 mg, 1.5 mmol) and BBr_3 (15 mL of 1 M solution in CH_2Cl_2) gave 381 mg (1.21 mmol, 81%) of white product. Calcd for $C_{18}H_{11}NO_4\cdot(H_2O)_{0.5}$ (MW 314.29): C, 68.79; H, 3.85; N, 4.46. Found: C, 68.32; H, 3.59; N, 4.32. EI MS *m/z*: 305 (100%, M^+). ^{1}H NMR (DMSO-d_6): δ 6.58 (dd, *J* 8.3, 2.5, 1H), 6.70 (d, *J* 2.5, 1H), 6.81 (d, *J* 8.6, 1H), 7.88 (t, *J* 7.7, 2H), 8.45–8.52 (m, 4H), 9.08–9.15 (m, 2H).

NDI. MeO-NDI (300 mg, 0.58 mmol) and BBr_3 (10 mL of 1.0 M solution in CH_2Cl_2) gave 184 mg (0.38 mmol, 65%) of yellow product. Calcd for $C_{28}H_{26}N_2O_6$ (M.W. 486.52): C, 69.12; H, 5.39; N, 5.76. Found: C, 68.88; H, 5.17; N, 5.56. EI MS *m/z*: 486 (100%, M^+). ^{1}H NMR (DMSO-d_6): δ 0.8–0.9 (m, br, 3H), 1.18–1.42 (m, br, 10H), 1.58–1.74 (m, br, 2H), 4.0–4.1 (t, br, 2H), 6.63 (dd, *J* 8.3, 2.1, 1H), 6.77 (d, *J* 1.5, 1H), 6.83 (d, *J* 8.3, 1H), 8.6–8.72 (m, 4H), 9.15–9.21 (m, 2H).

NAP-NDI. MeO-NAP-NDI (375 mg, 0.53 mmol) and BBr_3 (15 mL of 1 M solution in CH_2Cl_2) gave 275 mg (0.39 mmol, 73%) of dark-yellow product. Calcd for $C_{40}H_{31}N_3O_8\cdot(H_2O)_{1.5}$ (MW 708.71): C, 67.79; H, 4.84; N, 5.93. Found: C, 67.81; H, 4.32; N, 5.85. EI MS *m/z*: 681 (100%, M^+). ^{1}H NMR (DMSO-d_6): δ 0.81–0.9 (m, br, 3H), 1.2–1.45 (m, br, 10H), 1.6–1.75 (br, 2H), 4.01–4.13 (m, br, 2H), 6.63 (dd, *J* 8.3, 2.1, 1H), 6.77 (d, *J* 2.5, 1H), 6.83 (d, *J* 8.2, 1H), 7.96 (m, *J* 8.3, 7.3, 1H), 8.51–8.6 (m, 3H), 8.64 (d, *J* 1.8, 1H), 8.73 (s, 4H), 9.11–9.16 (m, br, 2H).

BTC. MeO-BTC (500 mg, 1.02 mmol) and BBr_3 (15 mL of 1 M solution in CH_2Cl_2) gave 369 mg (0.79 mmol, 77%) of yellow-orange product. Calcd for $C_{22}H_{12}N_2O_8\cdot(H_2O)_2$ (MW 468.37): C, 56.42; H, 3.44; N, 5.98. Found: C, 56.49; H, 2.87; N, 5.83. EI MS *m/z*: 432 (20%, M^+). ^{1}H NMR (DMSO-d_6): δ 6.72 (dd, *J* 8.3, 2.2, 2H), 6.82–6.88 (m, 4H), 8.28 (s, 2H), 9.27–9.33 (m, br, 4H).

Synthesis of Pt^{II} Diimine Complexes with Imide-Substituted Catechols, Pt(bpy*)(cat-imide). This reaction was not sensitive to the presence of moisture in the reagents or the solvents used. Pt(bpy*)Cl_2, the appropriate catechol, and $NaHCO_3$ (base) in 1:1:2 molar ratio were stirred at 95 °C in a degassed mixture of ethanol (10 mL) and DMF (2 mL) for 24 h under nitrogen. The reaction mixture was then cooled to RT and diluted with ether (50 mL or more) to give dark precipitate of the product that was filtered and washed with ether. The product was purified by column chromatography using 20 g of SiO_2 and 1.0% of CH_3OH in CH_2Cl_2 to remove minor red impurity and 1.5–2% of CH_3OH in CH_2Cl_2 to recover the product as a major red fraction. This fraction was reduced in volume to 5 mL, and the product was precipitated by addition of ether. The complexes were obtained as highly colored solids that were insoluble in alcohols, ether, and alkanes and were soluble in CH_2Cl_2, DMSO, and DMF.

Pt(bpy*)PHT. Pt(bpy*)Cl_2 (100 mg, 0.187 mmol), PHT (54.5 mg, 0.187 mmol), and $NaHCO_3$ (31 mg, 0.374 mmol) gave 95 mg (0.13 mmol, 69%) of blue product. Calcd for $C_{32}H_{31}N_3O_4Pt\cdot H_2O$ (MW 734.70): C, 52.31; H, 4.53; N, 5.72. Found: C, 52.47; H, 4.18; N, 5.66. ^{1}H NMR (DMSO-d_6): δ 1.42 (s, 9H), 1.43 (s, 9H), 6.26 (dd, *J* 8.3, 2.5, 1H), 6.45 (d, *J* 2.5, 1H), 6.56 (d, *J* 8.3, 1H),

7.73–7.80 (m, 2H), 7.83–7.95 (m, 4H), 8.60 (d, *J* 1.8, 2H), 8.93–9.02 (m, 2H).

Pt(bpy*)NAP. Pt(bpy*)Cl_2 (100 mg, 0.187 mmol), NAP (59 mg, 0.187 mmol), and $NaHCO_3$ (31 mg, 0.374 mmol) gave 99 mg (0.13 mmol, 69%) of blue product. Calcd for $C_{36}H_{33}N_3O_4Pt$ (M.W. 766.74): C, 56.39; H, 4.34; N, 5.48. Found: C, 55.98; H, 4.07; N, 5.10. ^{1}H NMR (DMSO-d_6): δ 1.42 (s, 9H), 1.44 (s, 9H), 6.18 (dd, *J* 8.3, 2.5, 1H), 6.39 (d, *J* 2.5, 1H), 6.56 (d, *J* 8.3, 1H), 7.74–7.81 (m, 2H), 7.88 (m, *J* 8.3, 7.3, 2H), 8.45–8.52 (m, 4H), 8.58–8.62 (m, 2H), 8.95–9.05 (m, 2H).

Pt(bpy*)NDI. Pt(bpy*)Cl_2 (55 mg, 0.10 mmol), NDI (50 mg, 0.10 mmol), and $NaHCO_3$ (17 mg, 0.20 mmol) gave 56 mg (0.06 mmol, 60%) of a deep blue product. Calcd for $C_{46}H_{48}N_4O_6Pt$ (MW 947.97): C, 58.28; H, 5.10; N, 5.91. Found: C, 57.58; H, 4.83; N, 5.61. ^{1}H NMR (DMSO-d_6): δ all signals were broad, 0.8–0.9 (m, 3H), 1.2–1.5 (m, 10H), 1.42 (s, 9H), 1.44 (s, 9H), 1.58–1.73 (m, 2H), 3.98–4.12 (m, 2H), 6.24 (dd, 1H), 6.44 (s, 1H), 6.58 (d, *J* 8.6, 1H), 7.72–7.81 (m, 2H), 8.61 (s, 2H), 8.67 (m, 4H), 8.91–9.05 (m, 2H).

Pt(bpy*)NAP-NDI. Pt(bpy*)Cl_2 (60 mg, 0.11 mmol), NAP-NDI (78 mg, 0.11 mmol), and $NaHCO_3$ (19 mg, 0.22 mmol) gave 91 mg (0.078 mmol, 71%) of deep violet product. Calcd for $C_{58}H_{53}N_5O_8Pt{\cdot}(H_2O)_{1.5}$ (MW 1170.17): C, 59.53; H, 4.82; N, 5.98. Found: C, 59.63; H, 4.56; N, 5.84. ^{1}H NMR ($CDCl_3$): δ 0.83–0.91 (m, 3H), 1.2–1.5 (m, br, 10H), 1.37 (s, 9H), 1.40 (s, 9H), 1.67–1.83 (br, 2H), 4.16–4.27 (m, 2H), 6.04 (d, *J* 2.1, 1H), 6.10 (dd, *J* 8.3, 2.5, 1H), 6.31 (d, *J* 8.2, 1H), 7.35–7.43 (m, 2H), 7.87 (t, *J* 7.4, 1H), 7.97 (d, *J* 1.5, 1H), 8.16 (d, *J* 1.5, 1H), 8.24 (d, *J* 2.1, 1H), 8.29 (dd, *J* 8.6, 0.9, 1H), 8.56 (d, *J* 2.2, 1H), 8.74 (dd, *J* 7.3, 1.2, 1H), 8.8–8.93 (m, 5H), 9.14 (d, *J* 6.4, 1H).

Synthesis of Pt(bpy*)(3,5-cat). This reaction was not sensitive to the presence of moisture in the reagents or the solvents used. Pt(bpy*)Cl_2 (80 mg, 0.15 mmol), 3,5-di-*tert*-butyl catechol (33 mg, 0.15 mmol), and KO^{t}Bu (34 mg, 0.30 mmol) were stirred at 90 °C in degassed ethanol (15 mL) for 24 h under nitrogen to give dark red solution. The reaction mixture was evaporated to dryness and was purified by column chromatography using 11 g of SiO_2 and 0.5% of CH_3OH in CH_2Cl_2 to remove impurities and 1.0% of CH_3OH in CH_2Cl_2 to recover the product as a major red fraction. This fraction was evaporated to dryness to give the product as a blue solid (89 mg, 0.13 mmol, 86%). Calcd for $C_{32}H_{44}N_2O_2Pt{\cdot}(H_2O)_{0.5}$ (MW 692.79): C, 55.48; H, 6.55; N, 4.04. Found: C, 55.23; H, 6.55; N, 4.04. ^{1}H NMR (acetone-d_6): δ 1.24 (s, 9H), 1.45 (s, 9H), 1.46 (s, 9H), 1.49 (s, 9H), 6.34 (d, *J* 2.2., 1H), 6.54 (d, *J* 2.5., 1H), 7.75 (dd, *J* 6.1, 2.1, 1H), 7.82 (dd, *J* 6.1, 2.2, 1H), 8.50 (d, *J* 2.2, 2H), 9.19 (dd, *J* 6.1, 0.6, 1H), 9.29 (dd, *J* 6.1, 0.6, 1H).

X-ray Crystallography. Single crystals were obtained by slow evaporation of CH_2Cl_2−2-methoxyethanol solution of Pt(bpy*)PHT and CH_2Cl_2−acetonitrile solution of Pt(bpy*)NAP.

Data were collected on a Bruker Smart CCD area detector with an Oxford Cryosystems low-temperature system. Reflections were measured from a hemisphere of data collected of frames each covering 0.5 degrees in Ω. All reflections were corrected for Lorentz and polarization effects and for absorption by semi empirical methods based on symmetry-equivalent and repeated reflections. The structure was solved by direct methods and refined by full matrix least-squares methods on F^2. Complex scattering factors were taken from the program package SHELXTL [An integrated system for solving and refining crystal structures from diffraction data, revision 5.1, Bruker AXS LTD] as implemented on an IBM PC. Hydrogen atoms were placed geometrically and refined with a riding model (including torsional freedom for methyl groups) and with U_{iso} constrained to be 1.2 (1.5 for methyl groups) times U_{eq} of the carrier atom. Data in common: T = 150(2) K; λ = 0.71073 Å.

Pt(bpy*)PHT:. $C_{32}H_{31}N_3O_4Pt{\cdot}(H_2O)_{0.5}$; MW 725.70; red blocks; size [mm] 0.21 × 0.18 × 0.12; space group *C*2/c; *a*/*b*/*c* [Å] = 25.7373(15)/16.6141(10)/15.1213(8); α/β/γ [deg] = 90/110.791(3)/90; V = 6044.8(6) Å^3; Z = 8; ρ_{calcd} = 1.595 g cm^{-3}; μ = 4.684 mm^{-1}; F(000) = 2872; θ range [deg] = 1.49–27.69; min/max transmission = 0.4396/0.6033; reflns collected/R_{int} = 29202/0.0791; data/restraints/params = 6981/257/363; GOF on F^2 = 0.972; R($I > 2\sigma I$) R1 = 0.0429, wR2 = 0.0918; R(all data) R1 = 0.0648, wR2 = 0.0978; $\Delta\rho_{min/max}$ [e Å^{-3}] = −1.670/2.231.

Pt(bpy*)NAP:. $C_{36}H_{33}N_3O_4Pt{\cdot}CH_3CN{\cdot}(H_2O)_{0.5}$; M.W. 816.81; red plates; size [mm] 0.46 × 0.10 × 0.03; monoclinic; space group *C*2/c (C_2^6 *h*, No. 15); *a*/*b*/*c* [Å] = 25.9691(12)/17.3615(8)/15.6346(7); α/β/γ [deg] = 90/110.836(2)/90; V = 6588.1(5) Å^3; Z = 8; ρ_{calcd} = 1.649 g cm^{-3}; μ = 4.309 mm^{-1}; F(000) = 3264; θ range [deg] = 1.44–32.35; min/max transmission = 0.2418/0.8816; reflns collected//R_{int} = 77538/0.0482; data/restraints/params = 11599/0/436; GOF on F^2 = 1.007; R($I > 2\sigma I$) R1 = 0.0278, wR2 = 0.0520; R(all data): R1 = 0.0537, wR2 = 0.0593; $\Delta\rho_{min/max}$ [e Å^{-3}] = −0.956/1.486.

Acknowledgment. We thank the Engineering and Physical Sciences Research Council (GR/T03352/02, GR/T03345/02), the EPSRC/RAL laser loan pool scheme, and the Royal Society for support, and Prof. M. D. Ward and Prof. D. Collison for fruitful discussions. J.B. thanks the CMSD CCLRC research network and the EPSRC CAN award for the provision of the studentship.

Note Added after ASAP Publication. This article was released ASAP on February 8, 2008, without its required CIF files. The correct version was posted on February 25, 2008.

Supporting Information Available: Absorption spectra of the catechols and Pt(bpy*)Cl_2 complex, absorption spectra of the neutral, oxidized, and reduced forms of the complexes Pt(bpy*)(cat-imide) (cat-imide = PHT, NAP, NDI) obtained from the spectroelectrochemical studies, cyclic voltammetry data for the complexes in DMF, and additional EPR spectra. Crystallographic data are available for Pt(bpy*)(NAP) (CCDC reference number 677818) and for Pt(bpy*)(PHT) (CCDC reference number 677819). This material is available free of charge via the Internet at http://pubs.acs.org.

IC701821D